
Exploring Adversarial Attacks against Latent Diffusion Model from the Perspective of Adversarial Transferability

Junxi Chen¹ Junhao Dong² Xiaohua Xie¹

Abstract

Recently, many studies utilized adversarial examples (AEs) to raise the cost of malicious image editing and copyright violation powered by latent diffusion models (LDMs). Despite their successes, a few have studied the surrogate model they used to generate AEs. In this paper, from the perspective of adversarial transferability, we investigate how the surrogate model’s property influences the performance of AEs for LDMs. Specifically, we view the time-step sampling in the Monte-Carlo-based (MC-based) adversarial attack as selecting surrogate models. We find that the smoothness of surrogate models at different time steps differs, and we substantially improve the performance of the MC-based AEs by selecting smoother surrogate models. In the light of the theoretical framework on adversarial transferability in image classification, we also conduct a theoretical analysis to explain why smooth surrogate models can also boost AEs for LDMs.

1. Introduction

Recently, latent diffusion models (LDMs) (Rombach et al., 2022), powered by the conditional mechanism and the low-cost diffusion process in low-dimensional latent space, have shown great flexibility in generating high-quality images with user-defined conditions and low computation overhead. However, just as every coin has two sides, the convenience and low budget of using LDMs also reduce the cost of malicious image generation. For example, an *adversary* can mimic the composition of a copyrighted photo by using image variation or can change someone’s behavior presented in the picture with the image inpainting.

¹School of Computer Science and Engineering, Sun Yat-sen University, Guangzhou, China ²School of Computer Science and Engineering, Nanyang Technological University, Singapore. Correspondence to: Xiaohua Xie <xiexiaoh6@mail.sysu.edu.cn>.

To prohibit the malicious usage of LDMs, some recent works (Liang et al., 2023; Salman et al., 2023; Zhang et al., 2023a; Liang & Wu, 2023) turned to adversarial examples (AEs) to protect the image from being edited or serving as a condition for image generation. They either added adversarial perturbations δ to push the image $x + \delta$ out of the generated distribution $p_\theta(x)$ (Liang et al., 2023) or disturbed the output (Salman et al., 2023) and intermediate latent (Liang & Wu, 2023; Zhang et al., 2023a) of LDMs in order to degrade the quality of the generated images.

In this paper, observing the inevitable discrepancy between the surrogate model used to manufacture AEs and the target model to attack, we model existing adversarial attacks to LDMs as transfer-based adversarial attacks. We investigate how the smoothness of the surrogate model, a significant factor affecting the adversarial transferability, influences the performance of AEs against LDMs.

Specifically, when generating AEs for LDMs, some adversarial attacks (Liang et al., 2023; Liang & Wu, 2023) use surrogate models different from the target model. Moreover, due to the variety of generation setups (e.g., guidance scale, prompt, and mask), the protected image faces multiple target models even if the adversary only uses one LDM for image editing. Consequently, adversarial transferability, meaning that AEs generated on one model can also crack other models, plays an important role. As a line of works improved the transferability empirically by modifying the surrogate model (Li et al., 2020; Springer et al., 2021; Gubri et al., 2022) and analyzed the relationship between the surrogate model and the transferability theoretically (Yang et al., 2021; Zhang et al., 2023b), studying AEs for LDMs from the perspective of the adversarial transferability and surrogate model may provide some hints for improving AEs’ performance.

Treating the time step as a part of the surrogate model’s weight, we view the time-step sampling in the MC-based adversarial attack (e.g., AdvDM) (Liang et al., 2023) as selecting surrogate models for manufacturing AEs. We find that the smoothness of surrogate models at different time steps varies, and such a discrepancy is significant enough to alter the performance of AEs. Empirical experiments demonstrate that limiting the sampling range of time steps

to where surrogate models are smooth can substantially improve AdvDM’s performance. Moreover, we conduct a theoretical study based on a theoretical framework (Yang et al., 2021; Zhang et al., 2023b) for adversarial transferability in the image classification task to explain why smoother surrogate models can also boost AEs for LDMs. Additionally, we find that AEs with good performance in corrupting image inpainting and variation may perform poorly in cracking image generation tasks requiring fine-tuning, e.g., textual inversion (Gal et al., 2023).

Our contributions are as follows.

- From the perspective of adversarial transferability and the smoothness of surrogate models, we conduct a theoretical study and empirical experiments to explain why limiting the sampling range of time steps in MC-based adversarial attacks works.
- Guided by our analyses and findings, we substantially improve MC-based AEs’ performance in cracking image inpainting and variation by simply limiting the sampling range of time steps.
- We find that AEs possessing good capability in corrupting image inpainting and image variation may not work well in degrading generation tasks requiring fine-tuning. Based on a very recent work (Wang et al., 2023), we explain why such a phenomenon exists, which reveals the differences and commonalities between AEs for these two types of tasks.

2. Preliminary

2.1. Diffusion Models and Latent Diffusion Models

The core of DM is the diffusion process. Specifically, given a sample $x_0 = x$, the diffusion process adds noise progressively to construct noisy samples x_1, x_2, \dots, x_T , where $x_t = \sqrt{\alpha_t}x_{t-1} + \sqrt{1 - \alpha_t}\epsilon$, and $\epsilon \sim \mathcal{N}(0, 1)$. This noise-adding process is commonly called the forward process. Such a progressive process can be transferred into a one-step process through reparameterization, where $x_t = \sqrt{\bar{\alpha}_t}x_0 + \sqrt{1 - \bar{\alpha}_t}\epsilon$, and $\bar{\alpha}_t = \prod_{i=1}^t \alpha_i$. To generate a new sample, the DM reverses the forward process and denoises x_t with the noise predicted by a denoising module $\epsilon_\theta(\cdot, t)$ at each step. The denoising module (usually an UNet) within the DM is trained by optimizing

$$\min_{\theta} \mathbb{E}_{x_0, t \sim u(t), \epsilon \sim \mathcal{N}(0, 1)} \|\epsilon - \epsilon_\theta(x_t, t)\|_2^2. \quad (1)$$

Rombach et al. (2022) proposed to conduct these two processes in relatively low-dimensional latent space and put forward the latent diffusion model (LDM) to reduce the overhead in training and sampling, where an encoder $\mathcal{E}(\cdot)$

is used to map the image to the latent space, and a decoder $\mathcal{D}(\cdot)$ maps the latent to the pixel space. We denote x_t as $\mathcal{A}(x, t) = \sqrt{\alpha_t}\mathcal{E}(x) + \sqrt{1 - \alpha_t}\epsilon$ to simplify the notation.

2.2. Inference Task and Fine-tuning Task

In this paper, we include two types of tasks, which are categorized into *inference* task and *fine-tuning* task.

The inference tasks we discuss include image variation and image inpainting (Rombach et al., 2022). Formally, these two tasks can be modeled as $f_{\text{infer}}(x, c') = \mathcal{D} \circ \epsilon_{t_1} \circ \dots \circ \epsilon_{t_n} \circ \mathcal{C}_{\text{infer}}(x, c')$, where $\mathcal{C}_{\text{infer}}$ extracts conditions from x without optimizing, and ϵ_t is the algorithm conducting denoising at step t . $f_{\text{infer}}(x, c')$ can be seen as an end-to-end inference model because no optimizing process is included and because $f_{\text{infer}}(x, c')$ is actually used as an end-to-end inference model by some adversarial attacks (Salman et al., 2023; Zhang et al., 2023a).

The fine-tuning task we discuss includes textual inversion (Gal et al., 2023). Formally, we model this task as $f_{\text{ft}}(x) = \mathcal{D} \circ \epsilon_{t_1} \circ \dots \circ \epsilon_{t_n} \circ \mathcal{C}_{\text{ft}}(x)$. Unlike the inference task, $f_{\text{ft}}(x)$ is not an end-to-end inference model because \mathcal{C}_{ft} is an algorithm extracting conditions from the image x by fine-tuning a pseudo word S^* .

2.3. Adversarial Examples for LDMs

AEs have been studied and utilized by many previous works (Liang et al., 2023; Salman et al., 2023; Le et al., 2023) to prohibit the malicious use of LDMs. They, *protectors*, optimize an adversarial perturbation δ within a space bounded by a budget ϵ and add the adversarial perturbation to an image x such that the *adversary* can not use this image as a condition to conduct generative tasks with LDMs. Formally, the goal of the protectors can be interpreted as

$$\max_{\delta} \mathcal{L}(f(x + \delta), y) \quad \text{s.t.} \quad \|\delta\|_p < \epsilon, \quad (2)$$

where y is a supervised signal, $f(\cdot)$ is the LDM specialized for an arbitrary task, and $\mathcal{L}(\cdot, \cdot)$ is a loss function. Intuitively, the objective of AEs for LDMs is to make the image generated by LDMs with the protected image being a condition unreal, and such unreality is measured by a loss function $\mathcal{L}(\cdot, \cdot)$.

In practice, an adversarial attack is designed to optimize a surrogate loss function with a surrogate model to raise the loss $\mathcal{L}(\cdot, \cdot)$. For better illustration, we categorize existing adversarial attacks on LDMs into three types: Encoder-based, chain-based, and Monte-Carlo-based (MC-based).

The encoder-based adversarial attack, first proposed by Salman et al. (2023), uses the encoder $\mathcal{E}(\cdot)$ within the LDM as its surrogate model. Formally, it crafts AEs by optimizing

$$\|\mathcal{E}(x + \delta) - \mathcal{E}(x_{\text{target}})\|_2^2 \quad \text{s.t.} \quad \|\delta\|_p < \epsilon, \quad (3)$$

where x_{targ} is a target image chosen by the protector. The key idea behind the encoder-based attack is to force the encoder to map the input image to some bad representation (Salman et al., 2023) and thus disrupt the image generation.

The chain-based adversarial attack (a.k.a diffusion attack (Salman et al., 2023)) includes the backward process of LDMs to simulate the inference of LDMs. Specifically, generating the chain-based targeted adversarial example (Salman et al., 2023) can be formulated as optimizing

$$\|f_{\text{infer}}(x + \delta, c) - x_{targ}\|_2^2 \quad \text{s.t.} \quad \|\delta\|_p < \varepsilon, \quad (4)$$

where c is the prompt and mask used during inference. In practice, the chain-based adversarial attack contains a long computation graph and thus induces a high computational cost.

The MC-based adversarial attack (a.k.a AdvDM) (Liang et al., 2023) constructs AEs on diffusion model by maximizing

$$\mathbb{E}_{t, \epsilon \sim \mathcal{N}(0,1)} \mathbb{E}_{x'_t \sim u(x'_t)} \left[\|\epsilon - \epsilon_\theta(x'_t, t)\|_2^2 \right], \quad (5)$$

where $x' = x + \delta$, $\|\delta\|_p < \varepsilon$, and the expectation is estimated by Monte Carlo. The MC-based adversarial attack aims to minimize the likelihood $p_\theta(x')$, which is opposite to the objective of the training process of LDMs. In practice, this algorithm can be seen as the training algorithm of LDMs with reversed loss function, where t is sampled from a uniform distribution $u(1, T)$, and δ is optimized by PGD (Madry et al., 2018) with gradient $\nabla_{x'} \|\epsilon - \epsilon_\theta(x'_t, t)\|_2^2$ at each step.

3. The Perspective of Transferability

In this section, we reformulate the MC-based adversarial attack as a transfer-based attack possessing a set of surrogate models. We conduct a theoretical study and claim that the MC-based adversarial example generated on smooth surrogate models is more potent than treating surrogate models equally because smoother surrogate models can improve adversarial transferability. We also conduct empirical experiments. We find that the smoothness of $\epsilon_{\theta \cup t}(\cdot)$ within LDMs differs. Thus, we can improve AEs' performance by picking the subset \mathcal{SM}' containing smoother $\epsilon_{\theta \cup t}(\cdot)$, which can support our findings and claims in the theoretical study.

3.1. Reformulating the MC-based adversarial attack

From Section 2.3, we can infer that the MC-based adversarial attack utilizes the denoising models $\epsilon_\theta(\cdot, t)$ as surrogate models and manages to crack $f_{\text{infer}}(\cdot)$. To some extent, the MC-based adversarial attack can be seen as a transfer-based adversarial attack because $f_{\text{infer}}(\cdot)$, the target model, is not included when manufacturing AEs.

Moreover, we can unfold $\epsilon_\theta(x_t, t)$ to $\epsilon_\theta(\sqrt{\bar{\alpha}_t}\mathcal{E}(x) + \sqrt{1 - \bar{\alpha}_t}\epsilon, t)$ ($\epsilon_{\theta \cup t}(x)$ for short) and treat t as a part of the denoising model's weight. In this sense, the protector owns a surrogate-model set $\mathcal{SM} = \{\epsilon_{\theta \cup t}(\cdot) \mid 1 \leq t \leq T\}$ rather than one surrogate model $\epsilon_\theta(\cdot, t)$ for constructing AEs. Consequently, if the property, e.g., smoothness, of the surrogate models in \mathcal{SM} varies, the protector can find a subset $\mathcal{SM}' \subseteq \mathcal{SM}$ such that one can generate better AEs with \mathcal{SM}' and attack LDMs more effectively.

3.2. Theoretical Study

The transferability of AEs has been studied theoretically in the image classification task (Yang et al., 2021; Zhang et al., 2023b). With modifications to definitions, we transfer a useful theorem on adversarial transferability in the image classification task to the image generation task. We only consider the untargeted attack.

Definition 3.1 (Model-dependent loss function). For a specific model \mathcal{F} , the loss function is defined as $\mathcal{L}_{\mathcal{F}}(x, y) : \mathcal{X} \times \mathcal{Y} \mapsto \mathbb{R}$, where x is the sample, and y is the supervised signal.

Definition 3.2 (β -Smooth). Given two arbitrary samples $x_1, x_2 \in \mathcal{X}$ and an arbitrary ground truth $y \in \mathcal{Y}$, a model \mathcal{F} is β -smooth if $\sup_{x_1, x_2, y} \frac{\|\nabla_{x_1} \mathcal{L}_{\mathcal{F}}(x_1, y) - \nabla_{x_2} \mathcal{L}_{\mathcal{F}}(x_2, y)\|_2}{\|x_1 - x_2\|} \leq \beta$.

Definition 3.3 (The risk and the empirical risk). Given a model \mathcal{F} and a loss value $L \in \mathbb{R}$, the model's *risk* is defined as $\gamma_{\mathcal{F}} = \Pr(\mathcal{L}_{\mathcal{F}}(x, y) > L)$. The model's *empirical risk* is defined as $\mathbb{E}_x [\mathcal{L}_{\mathcal{F}}(x, y)]$.

Definition 3.3 is one of the modifications to definitions compared to that of image classification task (Yang et al., 2021; Zhang et al., 2023b). Here, the risk is defined as the probability of the loss $\mathcal{L}_{\mathcal{F}}(x, y)$ being larger than a given value $L \in \mathbb{R}$.

Definition 3.4 ((α, \mathcal{F}) -Effective adversarial example). Given a model \mathcal{F} , an adversarial example x' is (α, \mathcal{F}) -effective if $\Pr(\mathcal{L}_{\mathcal{F}}(x', y) > L) \geq 1 - \alpha$.

Definition 3.5 (Loss gradient similarity). For two models \mathcal{F} and \mathcal{G} with loss functions $\mathcal{L}_{\mathcal{F}}$ and $\mathcal{L}_{\mathcal{G}}$, the loss gradient similarity is defined as $\mathcal{S}(\mathcal{L}_{\mathcal{F}}, \mathcal{L}_{\mathcal{G}}, x, y_1, y_2) = \frac{\nabla_x \mathcal{L}_{\mathcal{F}}(x, y_1) \cdot \nabla_x \mathcal{L}_{\mathcal{G}}(x, y_2)}{\|\nabla_x \mathcal{L}_{\mathcal{F}}(x, y_1)\|_2 \cdot \|\nabla_x \mathcal{L}_{\mathcal{G}}(x, y_2)\|_2}$.

The loss gradient similarity utilizes Cosine Similarity to measure the difference in loss gradients between two models. Following Zhang et al. (2023b), we further define the infimum of the loss gradient similarity as $\underline{\mathcal{S}}(\mathcal{L}_{\mathcal{F}}, \mathcal{L}_{\mathcal{G}}, x, y_1, y_2) = \inf_{x \in \mathcal{X}, y_1, y_2 \in \mathcal{Y}} \mathcal{S}(\mathcal{L}_{\mathcal{F}}, \mathcal{L}_{\mathcal{G}}, x, y_1, y_2)$.

Definition 3.6 (Adversarial transferability). For two models \mathcal{F} and \mathcal{G} with loss values $L_1, L_2 \in \mathbb{R}$, given a sample x ,

the transferability of the adversarial example $x' = x + \delta$ is defined as $T(\mathcal{F}, \mathcal{G}, x, y_1, y_2) = \mathbb{I}[\mathcal{L}_{\mathcal{F}}(x, y_1) \leq L_1 \wedge \mathcal{L}_{\mathcal{G}}(x, y_2) \leq L_2 \wedge \mathcal{L}_{\mathcal{F}}(x', y_1) > L_1 \wedge \mathcal{L}_{\mathcal{G}}(x', y_2) > L_2]$. \mathbb{I} is the indicator function.

Definition 3.6 is another key modification to definitions of previous works (Yang et al., 2021; Zhang et al., 2023b). Intuitively, high transferability means the adversarial example x' can effectively degrade the performance of both \mathcal{F} and \mathcal{G} .

Now, with modified definitions, we provide the lower bound of adversarial transferability.

Theorem 3.7 (The lower bound of adversarial transferability). *Assume the surrogate model \mathcal{F} and the target model \mathcal{G} are β -smooth. Given adversarial example $x' = x + \delta$ that is (α, \mathcal{F}) -Effective with $\|\delta\|_2 < \varepsilon \in \mathbb{R}$, the transferability can be lower bounded by*

$$\begin{aligned} Pr(T(\mathcal{F}, \mathcal{G}, x, y_1, y_2) = 1) &\geq (1 - \alpha) - \\ &(\gamma_{\mathcal{F}} + \gamma_{\mathcal{G}}) - \frac{\varepsilon(1 + \alpha) - c_{\mathcal{F}}(1 - \alpha)}{\varepsilon - c_{\mathcal{G}}} \\ &- \frac{\varepsilon(1 - \alpha)}{\varepsilon - c_{\mathcal{G}}} \sqrt{2 - 2\underline{\mathcal{S}}(\mathcal{L}_{\mathcal{F}}, \mathcal{L}_{\mathcal{G}}, x, y_1, y_2)}, \end{aligned} \quad (6)$$

where

$$c_{\mathcal{F}} = \min_{x \in \mathcal{D}} \frac{L_1 - \mathcal{L}_{\mathcal{F}}(x, y_1) - \beta\varepsilon^2/2}{\|\nabla_x \mathcal{L}_{\mathcal{F}}(x, y_1)\|_2}, \quad (7)$$

$$c_{\mathcal{G}} = \max_{x \in \mathcal{X}} \frac{L_2 - \mathcal{L}_{\mathcal{G}}(x, y_2) + \beta\varepsilon^2/2}{\|\nabla_x \mathcal{L}_{\mathcal{G}}(x, y_2)\|_2}, \quad (8)$$

$$\gamma_{\mathcal{F}} = Pr(\mathcal{L}_{\mathcal{F}}(x, y_1) > L_1), \quad (9)$$

$$\gamma_{\mathcal{G}} = Pr(\mathcal{L}_{\mathcal{G}}(x, y_2) > L_2), \quad (10)$$

and $L_1, L_2 \in \mathbb{R}$ and can be seen as constants.

The proof of Theorem 3.7 is provided in Appendix B. Note that, though Theorem 3.7 is based on l_2 -norm perturbation, one can trivially transfer Theorem 3.7 to l_{∞} -norm perturbation-based because $\|\delta\|_{\infty} < \varepsilon \Rightarrow \|\delta\|_2 < \sqrt{N} * \varepsilon$, where N is the number of components in δ .

Remark 3.8 (on Theorem 3.7). Theorem 3.7 can guide us to better manufacture the adversarial example from the perspective of the surrogate model’s smoothness. Specifically, regarding generating MC-based AEs for image inpainting and variation, we have

$$\mathcal{L}_{\mathcal{F}}(x, y) = \mathcal{L}_{\epsilon_{\theta \cup t}}(x, \epsilon) = \|\epsilon - \epsilon_{\theta \cup t}(x)\|_2, \quad (11)$$

and $\mathcal{L}_{\mathcal{G}}(x, y)$ can be

$$\mathcal{L}_{f_{\text{infer}}}(x, x_{\text{ori}}) = D(f_{\text{infer}}(x), x_{\text{ori}}), \quad (12)$$

where x_{ori} is the image to protect, and D is an arbitrary differentiable metric to measure the quality of the generated

image $f(x)$. We can infer from Equation (6) and Equation (7) that we can raise the lower bound of the adversarial transferability by decreasing β of the surrogate model, i.e., choosing a smooth surrogate model rather than a sharp one.

3.3. Empirical Study

Remark 3.8 demonstrates that we can improve the transferability by using smoother surrogate models. To confirm that this property can be applied to generating AEs for LDMS, we first conduct empirical experiments to measure the smoothness across different $\epsilon_{\theta \cup t}(\cdot)$ to see whether the smoothness differs according to t . Then, we partition \mathcal{SM} into several \mathcal{SM}' according to the smoothness of $\epsilon_{\theta \cup t}(\cdot)$ and construct AEs on each \mathcal{SM}' to examine if AEs generated on the \mathcal{SM}' containing smoother $\epsilon_{\theta \cup t}(\cdot)$ tend to have better performance. The setup of our empirical study is presented in Appendix A.1.

3.3.1. MEASURING SMOOTHNESS

To measure the smoothness of the $\epsilon_{\theta \cup t}(\cdot)$, we choose l_2 magnitude of gradients¹ (i.e., $\|\nabla_x \mathcal{L}_{\epsilon_{\theta \cup t}}(x, \epsilon)\|_2$) because the smoothness defined by Definition 3.2 is bounded by the l_2 magnitude of gradients (Yang et al., 2021).

In Figure 1, we can find that, on SD-v1-4 and SD-v1-5, the smoothness of $\epsilon_{\theta \cup t}(\cdot)$ decreases as t increases. In this case, choosing the $\epsilon_{\theta \cup t}(\cdot)$ with larger t should create AEs with better transferability and thus induce better protection to the image. On SD-v2-1, although the smoothness of $\epsilon_{\theta \cup t}(\cdot)$ also decreases and achieves its minimum when t is large, it is still much larger than that of the SD-v1-4 and the SD-v1-5.

Overall, Figure 1 supports our argument that t should be seen as a part of $\epsilon_{\theta}(\cdot, t)$ ’s weight as the property, e.g., smoothness, of $\epsilon_{\theta \cup t}(\cdot)$ within LDMS differs according to t . This finding motivates us to partition \mathcal{SM} by t and study the performance of AEs generated on each partition.

3.3.2. SMOOTHNESS CAN BOOST AEs FOR LDMS

The discussion and analysis in Section 3.3.1 show that the $\epsilon_{\theta \cup t}(\cdot)$ in SD-v1-4 and SD-v1-5 become smoother as t grows and that $\epsilon_{\theta \cup t}(\cdot)$ in SD-v2-1 are all relatively sharp. Based on our analysis in Section 3.2, we conjecture that AEs generated on $\epsilon_{\theta \cup t}(\cdot)$ with larger t in SD-v1-4 and SD-v1-5 are more effective in attacking LDMS. Also, due to the poor smoothness of $\epsilon_{\theta \cup t}(\cdot)$ in SD-v2-1, AEs generated on

¹We acknowledge that there are other metrics to measure the smoothness like the dominant eigenvalue of the Hessian matrix, used by Zhang et al. (2023b). However, the computation overhead of calculating the Hessian matrix of LDMS, where the input size is larger than that used by Zhang et al. (2023b), is overly large. We can not afford it even on A100.

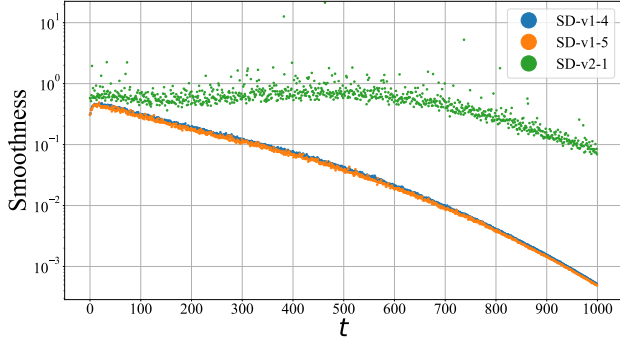


Figure 1. The smoothness of $\epsilon_{\theta_{Ut}}$ in different LDMs. Here, smoothness is measured by $\mathbb{E}_{x,\epsilon}[\|\nabla_x \mathcal{L}_{\epsilon_{\theta_{Ut}}}(x, \epsilon)\|_2]$. Lower the value of the y-axis, smoother the $\epsilon_{\theta_{Ut}}(\cdot)$ is.

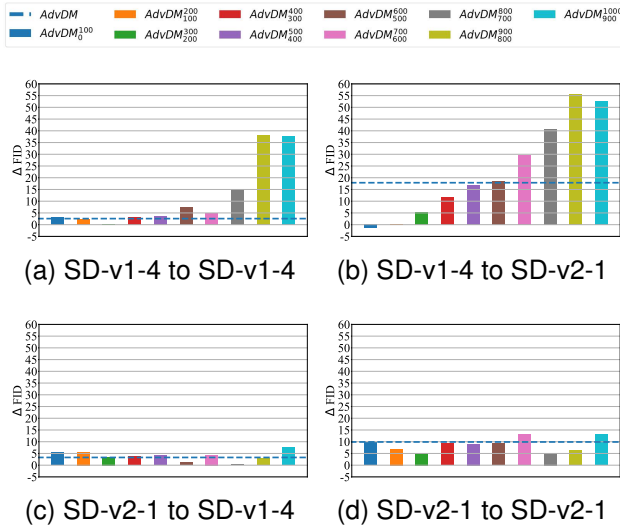


Figure 2. The increments \uparrow of FID relative to the benign’s. A larger increment means worse generated images and better AEs for breaking the image variation task. “A to B” means that AEs are generated by A and attack B.

SD-v2-1 should be relatively ineffective.

To validate our conjectures above, we partition \mathcal{SM} into 10 folds, where $\mathcal{SM}_a^b = \{\epsilon_{\theta_{Ut}}(\cdot) \mid a < t \leq b\}$, and test AEs generated on each fold by AdvDM (Liang et al., 2023) to examine whether the \mathcal{SM}_a^b containing smoother $\epsilon_{\theta_{Ut}}(\cdot)$ generates better AEs. For conciseness, we denote AdvDM using \mathcal{SM}_a^b as AdvDM $_a^b$ wherein AdvDM is AdvDM $_0^{1000}$. Following Liang et al. (2023) and Zhang et al. (2023a), we use FID (Heusel et al., 2017) to measure the effectiveness of AEs. We test AEs on image variation task and leave results on image inpainting in Appendix C. To save space, we only report the results of SD-v1-4 and SD-v2-1 and leave the results of other LDMs in Appendix C.

In Figure 2, we can find that AdvDM $_{800}^{900}$ and AdvDM $_{900}^{1000}$ can achieve larger increments of FID when AEs are generated on SD-v1-4, which means these AEs can effectively protect the images from being edited. Particularly in Figure 2(b), the increment of FID grows monotonically as a and b of AdvDM $_a^b$ become larger. These results are consistent with our conjectures because $\epsilon_{\theta_{Ut}}(\cdot)$ in SD-v1-4 tends to be smooth as t increases.

When the AE is generated on SD-v2-1, the differences in increments of FID between different methods are relatively minor, and AEs generated by $\epsilon_{\theta_{Ut}}(\cdot)$ with smaller t even have better performance (see Appendix C), which suggests that the smoothness of $\epsilon_{\theta_{Ut}}(\cdot)$ may be overwhelmed by other factors when the discrepancy of the smoothness is insignificant. This claim can also be supported by the results in Figure 2(a) and Figure 1, where the increments of FID remain low when t and the decline of $\mathbb{E}_{x,\epsilon}[\|\nabla_x \mathcal{L}_{\epsilon_{\theta_{Ut}}}(x, \epsilon)\|_2]$ is small.

One intriguing phenomenon in Figure 2(b) and Figure 2(d) is that, when t is large enough, AEs generated on SD-v1-4 are even more effective in attacking SD-v2-1 than those generated on SD-v2-1. This phenomenon demonstrates that choosing a smoother surrogate model can be better than choosing a surrogate model with the same weights as the target model when we try to crack LDMs. This phenomenon also supports our motivation that we should re-examine the adversarial attack for LDMs from the perspective of transferability because choosing the surrogate model having the same weights as the target model’s, which can be compared to white-box adversarial attack in image classification, does not ensure better performance.

4. Experiments

To demonstrate the effectiveness of our method, we compare the performance of AEs generated by our method to other SOTA adversarial attacks for LDMs. Considering that there exist other factors (e.g., iteration steps (Zhao et al., 2021) and gradient variance (Chen et al., 2023; Xiong et al., 2022)) affecting the performance of AEs, we conduct ablation studies in Section 4.3 to show that the performance gained by our method indeed comes from the smoothness of surrogate models. Lastly, we empirically show that a good AE for degrading image inpainting and variation is not necessarily a good AE for breaking textual inversion (Gal et al., 2023) and explain why such a phenomenon exists. We leave the setups of our experiments in Appendix A.2 and the results of AEs facing preprocessing adversarial defenses (Segura et al., 2023; Guo et al., 2018) in Appendix F. We also leave the results with SD-v1-5 being the surrogate model in Appendix D because its results are similar to SD-v1-4.

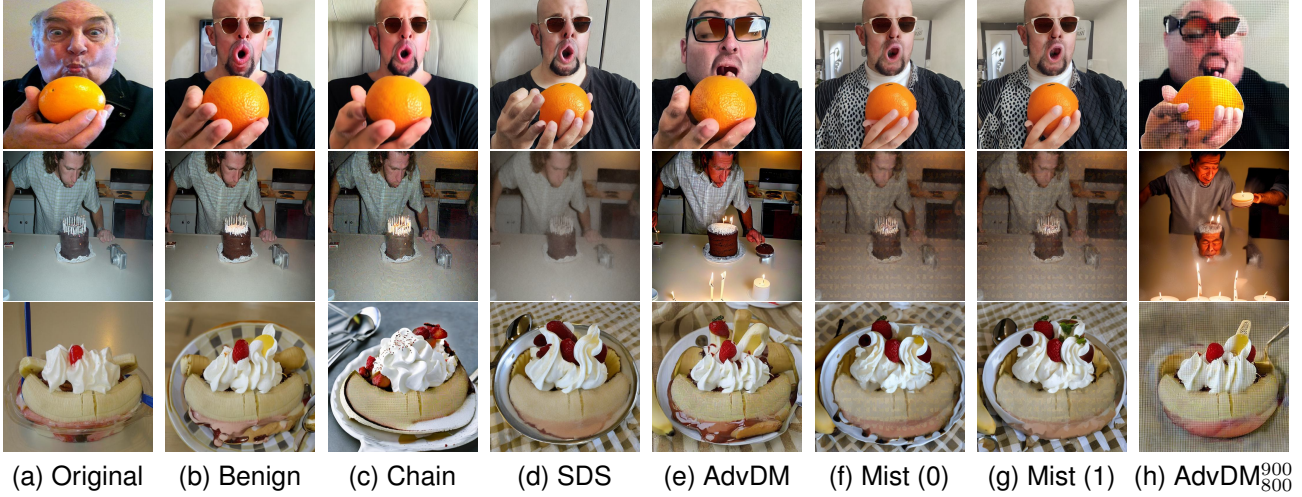


Figure 3. From top to bottom: Visualizations of image variation by SD-v1-4, image variation by InstructPix2Pix, and image inpainting by SD-2-Inpainting. Prompts from top to bottom: “A man holds a large orange and puckers up for a silly selfie.”, “On top of a brown cake, a man blows out white candles.”, and “A depiction of spoons and whipped cream on a classic banana split served in a traditional way.” View this figure in color. Use zoom-in to check the texture.

Table 1. The performance of AEs in corrupting image variation. The best result in each column is in bold.

Surrogate Model	Method	FID \uparrow				IS \downarrow				CLIP \downarrow				CLIP-IQA (Natural) \downarrow				CLIP-IQA (Noisiness) \downarrow			
		SD-v1-4	SD-v1-5	SD-v2-1	Instruct	SD-v1-4	SD-v1-5	SD-v2-1	Instruct	SD-v1-4	SD-v1-5	SD-v2-1	Instruct	SD-v1-4	SD-v1-5	SD-v2-1	Instruct	SD-v1-4	SD-v1-5	SD-v2-1	Instruct
/	Benign	164.28	166.51	195.82	130.41	16.60	16.06	11.25	16.39	34.47	34.61	32.38	34.53	0.45	0.46	0.27	0.32	0.47	0.48	0.38	0.36
SD-v1-4	AdvDM	166.86	173.84	213.68	180.03	15.29	15.29	9.56	15.06	34.65	34.45	31.24	34.22	0.45	0.44	0.18	0.22	0.44	0.44	0.27	0.39
	SDS	175.53	178.20	209.84	158.95	16.53	16.66	11.31	15.52	34.48	34.36	31.90	34.08	0.42	0.43	0.22	0.22	0.46	0.46	0.34	0.31
	Chain	182.40	178.99	228.90	162.77	12.87	13.11	8.10	15.62	33.85	34.01	30.07	34.46	0.36	0.37	0.14	0.22	0.39	0.41	0.21	0.34
	Mist (0)	181.72	181.69	233.38	156.41	16.07	15.28	8.82	15.47	34.17	34.02	30.53	34.02	0.43	0.44	0.19	0.17	0.46	0.46	0.33	0.17
	Mist (1)	181.39	181.32	232.41	157.93	15.88	15.05	8.42	14.54	34.10	34.09	30.43	33.82	0.44	0.43	0.19	0.17	0.46	0.46	0.32	0.17
	Mist (5)	166.87	168.44	214.75	182.16	16.00	15.93	9.92	15.51	34.61	34.53	31.09	34.20	0.45	0.47	0.21	0.22	0.44	0.44	0.30	0.39
	AdvDM ⁹⁰⁰ ₈₀₀	202.56	200.74	251.58	188.60	11.43	11.62	8.08	15.26	33.52	33.71	29.63	33.93	0.30	0.31	0.09	0.22	0.31	0.32	0.16	0.41
	Mist ⁹⁰⁰ ₈₀₀ (1)	184.22	181.84	231.27	155.76	16.15	15.28	8.89	14.97	34.20	34.09	30.44	33.98	0.44	0.45	0.20	0.18	0.46	0.47	0.32	0.17
Mist ⁹⁰⁰ ₈₀₀ (5)	204.46	199.11	251.94	188.47	12.11	12.26	7.15	14.83	33.69	33.83	29.67	33.95	0.30	0.32	0.09	0.21	0.32	0.34	0.16	0.41	
SD-v2-1	AdvDM	167.58	167.57	205.71	158.43	16.49	16.26	10.81	16.66	34.45	34.50	31.63	34.46	0.44	0.43	0.24	0.22	0.46	0.46	0.33	0.31
	SDS	165.58	166.92	197.62	164.52	15.56	15.04	11.28	16.14	34.41	34.44	31.93	34.38	0.35	0.36	0.20	0.23	0.42	0.42	0.29	0.35
	Chain	169.05	169.11	209.25	142.08	16.41	15.98	10.19	16.33	34.66	34.39	30.84	34.61	0.43	0.48	0.23	0.24	0.43	0.45	0.25	0.28
	Mist (0)	182.05	181.88	231.28	158.82	15.83	15.12	8.75	15.02	34.20	34.06	30.54	33.90	0.43	0.44	0.20	0.18	0.46	0.45	0.33	0.17
	Mist (1)	179.14	179.71	227.45	139.39	16.07	15.26	8.94	15.81	34.24	34.31	30.85	34.18	0.44	0.45	0.22	0.21	0.45	0.46	0.33	0.20
	Mist (5)	165.70	167.17	205.23	159.58	16.95	16.84	10.89	16.52	34.35	34.47	31.75	34.53	0.45	0.45	0.23	0.22	0.45	0.46	0.32	0.33
	AdvDM ⁹⁰⁰ ₈₀₀	167.19	169.71	202.05	160.66	15.13	16.12	11.77	16.18	34.33	34.34	31.99	34.38	0.39	0.39	0.24	0.22	0.44	0.46	0.30	0.35
	Mist ⁹⁰⁰ ₈₀₀ (1)	179.03	181.39	236.64	148.00	15.81	15.13	8.58	15.21	34.05	34.05	30.13	34.17	0.44	0.44	0.19	0.19	0.47	0.48	0.29	0.19
Mist ⁹⁰⁰ ₈₀₀ (5)	168.08	167.66	201.62	161.90	15.73	15.82	11.89	15.87	34.19	34.32	31.91	34.33	0.39	0.39	0.23	0.23	0.45	0.46	0.31	0.34	

4.1. Qualitative Results

To intuitively demonstrate how different adversarial attacks corrupt the image variation and inpainting, we visualize the generated images in Figure 3. When attacking SD-v1-4 and SD-2-Inpainting, one significant pattern induced by AdvDM⁹⁰⁰₈₀₀ is the latticed texture across the whole image. This pattern makes the generated images noisy, unreal, and lacking depth of field. Among the images generated by InstructPix2Pix, the image of AdvDM⁹⁰⁰₈₀₀ fails to mimic the composition and the objects in the original image, where the cake becomes a head, and candles are burning above the head. Other methods, like Chain, SDS, and Mist, introduce noise, blurriness, and the pattern from the target image to the generated image, respectively. We present more visualizations in Appendix G.

4.2. Quantitative Results

We quantitatively evaluate the performance of AEs from three perspectives, including preventing imitations, biasing the semantics provided by the prompt, and degrading the visual quality (see Appendix A.2).

In Table 1 and Table 2, we can find that the best results are achieved mainly by AdvDM⁹⁰⁰₈₀₀ or Mist⁹⁰⁰₈₀₀(5). Specifically, AEs generated by Mist⁹⁰⁰₈₀₀ with SD-v1-4 being the surrogate model induce higher FID than other methods, suggesting that the generated images’ distribution differs from the original images’. Thus, the adversary may fail to mimic the protected images. Regarding biasing the semantics provided by prompts, AdvDM⁹⁰⁰₈₀₀ and Mist⁹⁰⁰₈₀₀ tend to have low CLIP values, indicating that the generated images have different semantics from the prompts. In practice, this property can hinder the adversary from generating images fulfilling

Table 2. The performance of AEs in corrupting image inpainting. The best result in each column is in **bold**.

Surrogate Model	Method	FID \uparrow		IS \downarrow		CLIP \downarrow		CLIP-IQA (Natural) \downarrow		CLIP-IQA (Noisiness) \downarrow	
		SD-Inpainting	SD-2-Inpainting	SD-Inpainting	SD-2-Inpainting	SD-Inpainting	SD-2-Inpainting	SD-Inpainting	SD-2-Inpainting	SD-Inpainting	SD-2-Inpainting
/	Benign	108.04	105.79	15.67	16.64	34.58	34.93	0.47	0.53	0.43	0.45
SD-v1-4	AdvDM	145.78	143.18	14.61	14.86	34.37	34.85	0.23	0.25	0.35	0.32
	SDS	142.93	147.80	15.19	16.09	34.56	35.00	0.35	0.34	0.36	0.27
	Mist (0)	156.25	163.67	13.90	14.75	34.02	34.17	0.25	0.22	0.36	0.30
	Mist (1)	157.43	162.91	14.47	14.69	34.04	34.30	0.24	0.21	0.37	0.29
	Mist (5)	145.68	142.33	14.18	15.13	34.44	35.04	0.25	0.27	0.35	0.32
	AdvDM $_{800}^{900}$	161.83	168.86	13.18	12.79	34.18	34.66	0.21	0.21	0.26	0.23
	Mist $_{800}^{900}$ (1)	158.27	163.56	14.13	14.89	33.97	34.23	0.24	0.22	0.38	0.30
	Mist $_{800}^{900}$ (5)	161.11	169.32	14.23	12.58	34.21	34.54	0.21	0.22	0.28	0.23
SD-v2-1	AdvDM	126.19	128.06	15.32	17.29	34.68	34.85	0.35	0.36	0.39	0.38
	SDS	122.36	122.96	14.63	15.75	34.36	34.60	0.35	0.36	0.38	0.35
	Mist (0)	153.58	162.56	14.20	14.20	34.03	34.21	0.25	0.21	0.37	0.28
	Mist (1)	146.19	149.69	15.61	16.38	34.48	34.54	0.28	0.26	0.38	0.32
	Mist (5)	124.32	130.38	15.66	16.48	34.47	34.77	0.35	0.38	0.39	0.38
	AdvDM $_{800}^{900}$	123.76	123.33	16.51	15.62	34.42	34.76	0.36	0.39	0.38	0.36
	Mist $_{800}^{900}$ (1)	150.37	152.98	14.84	14.86	34.09	34.33	0.26	0.25	0.39	0.32
	Mist $_{800}^{900}$ (5)	120.26	120.34	16.78	15.57	34.33	34.66	0.37	0.38	0.39	0.36
SD-Inpainting	Chain	151.68	147.03	14.83	14.49	33.82	34.30	0.25	0.26	0.33	0.33
SD-2-Inpainting	Chain	154.01	149.47	14.94	14.55	34.10	34.49	0.23	0.26	0.34	0.37

Table 3. The performance of AEs generated by AdvDM (Liang et al., 2023) and AdvDM $_{800}^{900}$ with different iteration steps in cracking image variation. The surrogate model is SD-v1-4.

Method	Iteration Steps	FID \uparrow				IS \downarrow			
		SD-v1-4	SD-v1-5	SD-v2-1	Instruct	SD-v1-4	SD-v1-5	SD-v2-1	Instruct
AdvDM	40	166.86	173.84	213.68	180.03	15.29	15.29	9.56	15.06
	500	170.74	173.84	225.97	185.13	15.68	15.29	9.19	15.19
	1,000	173.77	171.11	230.73	184.93	15.30	15.17	9.22	15.29
AdvDM $_{800}^{900}$	40	202.56	200.74	251.58	188.60	11.43	11.62	8.08	15.26
	500	243.93	242.59	279.78	192.93	7.08	7.71	6.17	14.02

its purpose.

As for degrading the generated images’ quality, AdvDM $_{800}^{900}$ and Mist $_{800}^{900}$ (5) also lead to low IS and CLIP-IQA values when attacking LDMs except for InstructPix2Pix. Significantly, the values of CLIP-IQA demonstrate that AdvDM $_{800}^{900}$ introduce more unnatural and noisy patterns into the generated images, which is consistent with our observation in Section 4.1. When attacking InstructPix2Pix, as we observe in Section 4.1, AdvDM $_{800}^{900}$ corrupts the image variation by biasing the semantics of the generated image rather than degrading the visual quality, which leads to relatively high FID and CLIP-IQA values.

Also, as we claimed in Section 3.3.2, SD-v2-1 is not a good surrogate model for manufacturing MC-based AEs. All MC-based AEs constructed on SD-v2-1 have poorer performance than those constructed on SD-v1-4. Only Mist (0), an encoder-based adversarial attack, can achieve similar results across these two surrogate models.

4.3. Ablation Study

4.3.1. ITERATION STEPS

Zhao et al. (2021) find that the adversarial attack with only a few iterations has limited the attack convergence to optimal targeted transferability. Liang et al. (2023) also improves AdvDM’s performance by including more iteration steps. These findings inspire us to check whether the improvement

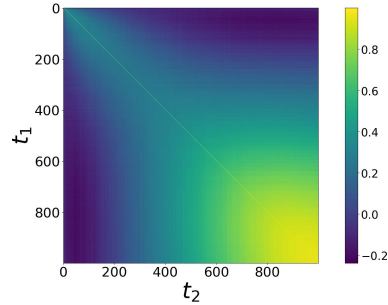


Figure 4. The loss gradient similarity matrix of SD-v1-4. The value of position (t_1, t_2) is $\mathbb{E}_{x, \epsilon_1, \epsilon_2} \mathcal{S}(\mathcal{L}_{\epsilon_{\theta} U_{t_1}}, \mathcal{L}_{\epsilon_{\theta} U_{t_2}}, x, \epsilon_1, \epsilon_2)$.

Table 4. The performance of AEs generated by AdvDM $_{99}^{100}$, AdvDM $_{499}^{500}$, and AdvDM $_{999}^{1000}$ in cracking image variation. The surrogate model is SD-v1-4.

Method	FID \uparrow				IS \downarrow			
	SD-v1-4	SD-v1-5	SD-v2-1	Instruct	SD-v1-4	SD-v1-5	SD-v2-1	Instruct
AdvDM $_{99}^{100}$	166.08	165.58	195.41	168.37	16.5	16.21	11.66	16.53
AdvDM $_{499}^{500}$	169.13	168.57	213.9	179.48	16.46	15.75	10.25	16.03
AdvDM $_{999}^{1000}$	195.62	193.11	243.57	188.71	12.64	12.18	7.66	15.34

gained by our method comes from a faster convergence rate rather than the smoothness. We set the iteration steps of AdvDM to at most 1,000 to ensure convergence. In Table 3, we can find that increasing iteration steps can boost the performance of AEs but still can not surpass AdvDM $_{800}^{900}$ with 40 iteration steps. This result demonstrates that the adversarial perturbation generated by AdvDM $_{800}^{900}$ converges to a more optimum point. Moreover, the performance of AdvDM $_{800}^{900}$ can also be improved by incorporating more iteration steps, indicating that the performance of AdvDM $_{800}^{900}$ is not gained by a faster convergence rate. We present the results of different adversarial attacks with 500 iteration steps and different inference tasks in Appendix E.

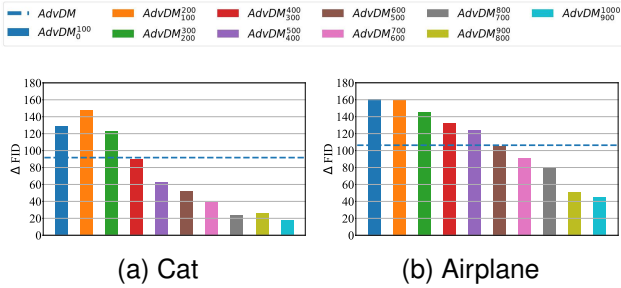


Figure 5. The increments \uparrow of FID relative to the benign’s. Larger increment means worse generated images and better AEs for textual inversion.

4.3.2. GRADIENT VARIANCE

We mentioned in Section 3 that, to some extent, the MC-based adversarial attack owns a surrogate-model set rather than one surrogate model for constructing AEs, which makes the MC-based adversarial attack an ensemble-based attack (Chen et al., 2023; Xiong et al., 2022). Xiong et al. (2022) claimed the low loss gradient similarity between surrogate models would degrade the performance of AEs. Thus, we need to confirm whether this factor, rather than smoothness, dominates the performance of AEs.

We measure the loss gradient similarity between $\epsilon_{\theta_{Ut}}(\cdot)$ with different t (see Figure 4) and find that the loss gradient similarity within \mathcal{SM}_t^{t+l} increases as t grows. To eliminate the discrepancy of the loss gradient similarity, we set l to 1. We then construct MC-based AEs on \mathcal{SM}_t^{t+1} and test these AEs. In Table 4, we find that AdvDM₉₉₉¹⁰⁰⁰, which uses smoother $\epsilon_{\theta_{Ut}}(\cdot)$, generates far better AEs than AdvDM₄₉₉⁵⁰⁰ and AdvDM₉₉¹⁰⁰. This result demonstrates that higher loss gradient similarity is not the main factor improving the performance of AdvDM_t^{t+100} with larger t .

4.4. Fine-tuning Task

We also test the performance of AEs generated on different \mathcal{SM}_a^b in disrupting textual inversion. In Figure 5, we can find that the performance of AEs generated on \mathcal{SM}_a^b with larger a and b is worse, which is contrary to the results of image variation and inpainting. We mentioned in Section 2.2 that the fine-tuning task can not be seen as an end-to-end inference model because the fine-tuning task includes an optimizing process. In this sense, AEs for cracking the fine-tuning task act as poisoned data (Huang et al., 2021; Fowl et al., 2021) rather than carriers for adversarial attacks (Goodfellow et al., 2015). Consequently, our analysis based on end-to-end inference models can not explain the results of the fine-tuning task.

One reasonable explanation comes from a very recent work (Wang et al., 2023). Wang et al. (2023) found that

$\epsilon_{\theta_{Ut}}(\cdot)$ with smaller t focuses on the higher frequency components of images while $\epsilon_{\theta_{Ut}}(\cdot)$ with larger t focuses on the lower frequency. Wang et al. (2023) claimed that introducing adversarial noises at larger time steps is ineffective because the subtle changes perturbed on images can hardly affect the low-frequency of the generated images. These findings may explain why sampling larger t can not boost AEs for textual inversion. Moreover, these findings can also explain the results in Figure 7(c) and Figure 7(f), where the performance of AEs generated on SD-v2-1 degrades as t grows, because the smoothness of SD-v2-1 does not alter significantly over t . This property allows the factor found by Wang et al. (2023) to dominate the results.

5. Conclusion

In this paper, we model the MC-based adversarial attack for the inference task as a transfer-based adversarial attack wherein the property of the surrogate model significantly impacts the adversarial transferability. We view the time-step sampling in AdvDM (Liang et al., 2023) as selecting different surrogate models and find that the smoothness of surrogate models at different time steps varies. In some LDMs, such variety is influential enough to alter the performance of AdvDM. We limit the range of time-step sampling to where surrogate models are smooth and boost the performance of AdvDM. Based on the theoretical framework (Yang et al., 2021; Zhang et al., 2023b) for adversarial transferability in the image classification task, we conduct a theoretical study and claim that smooth surrogate models can also improve the performance of AEs for LDMs. Moreover, AEs with better performance in breaking the inference task may not work well in cracking the fine-tuning task, revealing the discrepancy and commonalities between AEs for the inference task and the fine-tuning task.

References

- Bianchi, F., Attanasio, G., Pisoni, R., Terragni, S., Sarti, G., and Lakshmi, S. Contrastive language-image pre-training for the italian language. *CoRR*, abs/2108.08688, 2021. URL <https://arxiv.org/abs/2108.08688>.
- Chen, B., Yin, J., Chen, S., Chen, B., and Liu, X. An adaptive model ensemble adversarial attack for boosting adversarial transferability. *CoRR*, abs/2308.02897, 2023. doi: 10.48550/ARXIV.2308.02897. URL <https://doi.org/10.48550/arXiv.2308.02897>.
- Fowl, L., Goldblum, M., Chiang, P., Geiping, J., Czaja, W., and Goldstein, T. Adversarial examples make strong poisons. In Ranzato, M., Beygelzimer, A., Dauphin, Y. N., Liang, P., and Vaughan, J. W. (eds.), *Advances in Neural Information Processing Systems 34: Annual Conference on Neural Information Processing Systems 2021*,

- NeurIPS 2021, December 6-14, 2021, virtual*, pp. 30339–30351, 2021. URL <https://proceedings.neurips.cc/paper/2021/hash/fe87435d12ef7642af67d9bc82a8b3cd-Abstract./openreview.net/forum?id=iAmZUo0DxC0.html>.
- Gal, R., Alaluf, Y., Atzmon, Y., Patashnik, O., Bermano, A. H., Chechik, G., and Cohen-Or, D. An image is worth one word: Personalizing text-to-image generation using textual inversion. In *The Eleventh International Conference on Learning Representations, ICLR 2023, Kigali, Rwanda, May 1-5, 2023*. OpenReview.net, 2023. URL <https://openreview.net/pdf?id=NAQvF08TcyG>.
- Goodfellow, I. J., Shlens, J., and Szegedy, C. Explaining and harnessing adversarial examples. In Bengio, Y. and LeCun, Y. (eds.), *3rd International Conference on Learning Representations, ICLR 2015, San Diego, CA, USA, May 7-9, 2015, Conference Track Proceedings*, 2015. URL <http://arxiv.org/abs/1412.6572>.
- Gubri, M., Cordy, M., Papadakis, M., Traon, Y. L., and Sen, K. LGV: boosting adversarial example transferability from large geometric vicinity. In Avidan, S., Brostow, G. J., Cissé, M., Farinella, G. M., and Hassner, T. (eds.), *Computer Vision - ECCV 2022 - 17th European Conference, Tel Aviv, Israel, October 23-27, 2022, Proceedings, Part IV*, volume 13664 of *Lecture Notes in Computer Science*, pp. 603–618. Springer, 2022. doi: 10.1007/978-3-031-19772-7_35. URL https://doi.org/10.1007/978-3-031-19772-7_35.
- Guo, C., Rana, M., Cissé, M., and van der Maaten, L. Countering adversarial images using input transformations. In *6th International Conference on Learning Representations, ICLR 2018, Vancouver, BC, Canada, April 30 - May 3, 2018, Conference Track Proceedings*. OpenReview.net, 2018. URL <https://openreview.net/forum?id=SyJ7C1WCB>.
- Heusel, M., Ramsauer, H., Unterthiner, T., Nessler, B., and Hochreiter, S. Gans trained by a two time-scale update rule converge to a local nash equilibrium. In Guyon, I., von Luxburg, U., Bengio, S., Wallach, H. M., Fergus, R., Vishwanathan, S. V. N., and Garnett, R. (eds.), *Advances in Neural Information Processing Systems 30: Annual Conference on Neural Information Processing Systems 2017, December 4-9, 2017, Long Beach, CA, USA*, pp. 6626–6637, 2017. URL <https://proceedings.neurips.cc/paper/2017/hash/8a1d694707eb0fefe65871369074926d-Abstract.html>.
- Huang, H., Ma, X., Erfani, S. M., Bailey, J., and Wang, Y. Unlearnable examples: Making personal data unexploitable. In *9th International Conference on Learning Representations, ICLR 2021, Virtual Event, Austria, May 3-7, 2021*. OpenReview.net, 2021. URL <https://openreview.net/forum?id=iAmZUo0DxC0>.
- Le, T. V., Phung, H., Nguyen, T. H., Dao, Q., Tran, N., and Tran, A. Anti-dreambooth: Protecting users from personalized text-to-image synthesis. *CoRR*, abs/2303.15433, 2023. doi: 10.48550/ARXIV.2303.15433. URL <https://doi.org/10.48550/arXiv.2303.15433>.
- Li, Y., Bai, S., Zhou, Y., Xie, C., Zhang, Z., and Yuille, A. L. Learning transferable adversarial examples via ghost networks. In *The Thirty-Fourth AAAI Conference on Artificial Intelligence, AAAI 2020, The Thirty-Second Innovative Applications of Artificial Intelligence Conference, IAAI 2020, The Tenth AAAI Symposium on Educational Advances in Artificial Intelligence, EAAI 2020, New York, NY, USA, February 7-12, 2020*, pp. 11458–11465. AAAI Press, 2020. doi: 10.1609/AAAI.V34I07.6810. URL <https://doi.org/10.1609/aaai.v34i07.6810>.
- Liang, C. and Wu, X. Mist: Towards improved adversarial examples for diffusion models. *CoRR*, abs/2305.12683, 2023. doi: 10.48550/ARXIV.2305.12683. URL <https://doi.org/10.48550/arXiv.2305.12683>.
- Liang, C., Wu, X., Hua, Y., Zhang, J., Xue, Y., Song, T., Xue, Z., Ma, R., and Guan, H. Adversarial example does good: Preventing painting imitation from diffusion models via adversarial examples. In Krause, A., Brunskill, E., Cho, K., Engelhardt, B., Sabato, S., and Scarlett, J. (eds.), *International Conference on Machine Learning, ICML 2023, 23-29 July 2023, Honolulu, Hawaii, USA*, volume 202 of *Proceedings of Machine Learning Research*, pp. 20763–20786. PMLR, 2023. URL <https://proceedings.mlr.press/v202/liang23g.html>.
- Madry, A., Makelov, A., Schmidt, L., Tsipras, D., and Vladu, A. Towards deep learning models resistant to adversarial attacks. In *6th International Conference on Learning Representations, ICLR 2018, Vancouver, BC, Canada, April 30 - May 3, 2018, Conference Track Proceedings*. OpenReview.net, 2018. URL <https://openreview.net/forum?id=rJzIBfZAb>.
- Rombach, R., Blattmann, A., Lorenz, D., Esser, P., and Ommer, B. High-resolution image synthesis with latent diffusion models. In *IEEE/CVF Conference on Computer Vision and Pattern Recognition, CVPR 2022, New Orleans, LA, USA, June 18-24, 2022*, pp. 10674–10685. IEEE, 2022. doi: 10.1109/CVPR52688.2022.01042. URL <https://doi.org/10.1109/CVPR52688.2022.01042>.

- Salimans, T., Goodfellow, I. J., Zaremba, W., Cheung, V., Radford, A., and Chen, X. Improved techniques for training gans. In Lee, D. D., Sugiyama, M., von Luxburg, U., Guyon, I., and Garnett, R. (eds.), *Advances in Neural Information Processing Systems 29: Annual Conference on Neural Information Processing Systems 2016, December 5-10, 2016, Barcelona, Spain*, pp. 2226–2234, 2016. URL <https://proceedings.neurips.cc/paper/2016/hash/8a3363abe792db2d8761d6403605aeb7-Abstract.html>.
- Salman, H., Khaddaj, A., Leclerc, G., Ilyas, A., and Madry, A. Raising the cost of malicious ai-powered image editing. In Krause, A., Brunskill, E., Cho, K., Engelhardt, B., Sabato, S., and Scarlett, J. (eds.), *International Conference on Machine Learning, ICML 2023, 23-29 July 2023, Honolulu, Hawaii, USA*, volume 202 of *Proceedings of Machine Learning Research*, pp. 29894–29918. PMLR, 2023. URL <https://proceedings.mlr.press/v202/salman23a.html>.
- Segura, P. S., Geiping, J., and Goldstein, T. JPEG compressed images can bypass protections against AI editing. *CoRR*, abs/2304.02234, 2023. doi: 10.48550/ARXIV.2304.02234. URL <https://doi.org/10.48550/arXiv.2304.02234>.
- Springer, J. M., Mitchell, M., and Kenyon, G. T. A little robustness goes a long way: Leveraging robust features for targeted transfer attacks. In Ranzato, M., Beygelzimer, A., Dauphin, Y. N., Liang, P., and Vaughan, J. W. (eds.), *Advances in Neural Information Processing Systems 34: Annual Conference on Neural Information Processing Systems 2021, NeurIPS 2021, December 6-14, 2021, virtual*, pp. 9759–9773, 2021. URL <https://proceedings.neurips.cc/paper/2021/hash/50f3f8c42b998a48057e9d33f4144b8b-Abstract.html>.
- von Platen, P., Patil, S., Lozhkov, A., Cuenca, P., Lambert, N., Rasul, K., Davaadorj, M., and Wolf, T. Diffusers: State-of-the-art diffusion models. <https://github.com/huggingface/diffusers>, 2022.
- Wang, F., Tan, Z., Wei, T., Wu, Y., and Huang, Q. SimAC: A Simple Anti-Customization Method against Text-to-Image Synthesis of Diffusion Models. *arXiv e-prints*, art. arXiv:2312.07865, December 2023. doi: 10.48550/arXiv.2312.07865.
- Wang, J., Chan, K. C. K., and Loy, C. C. Exploring CLIP for assessing the look and feel of images. In Williams, B., Chen, Y., and Neville, J. (eds.), *Thirty-Seventh AAAI Conference on Artificial Intelligence, AAAI 2023, Thirty-Fifth Conference on Innovative Applications of Artificial Intelligence, IAAI 2023, Thirteenth Symposium on Educational Advances in Artificial Intelligence, EAAI 2023, Washington, DC, USA, February 7-14, 2023*, pp. 2555–2563. AAAI Press, 2023. doi: 10.1609/AAAI.V37I2.25353. URL <https://doi.org/10.1609/aaai.v37i2.25353>.
- Xiong, Y., Lin, J., Zhang, M., Hopcroft, J. E., and He, K. Stochastic variance reduced ensemble adversarial attack for boosting the adversarial transferability. In *IEEE/CVF Conference on Computer Vision and Pattern Recognition, CVPR 2022, New Orleans, LA, USA, June 18-24, 2022*, pp. 14963–14972. IEEE, 2022. doi: 10.1109/CVPR52688.2022.01456. URL <https://doi.org/10.1109/CVPR52688.2022.01456>.
- Xue, H., Liang, C., Wu, X., and Chen, Y. Toward effective protection against diffusion based mimicry through score distillation. *CoRR*, abs/2311.12832, 2023. doi: 10.48550/ARXIV.2311.12832. URL <https://doi.org/10.48550/arXiv.2311.12832>.
- Yang, Z., Li, L., Xu, X., Zuo, S., Chen, Q., Zhou, P., Rubinstein, B. I. P., Zhang, C., and Li, B. TRS: transferability reduced ensemble via promoting gradient diversity and model smoothness. In Ranzato, M., Beygelzimer, A., Dauphin, Y. N., Liang, P., and Vaughan, J. W. (eds.), *Advances in Neural Information Processing Systems 34: Annual Conference on Neural Information Processing Systems 2021, NeurIPS 2021, December 6-14, 2021, virtual*, pp. 17642–17655, 2021. URL <https://proceedings.neurips.cc/paper/2021/hash/937936029af671cf479fa893db91cbdd-Abstract.html>.
- Yu, F., Zhang, Y., Song, S., Seff, A., and Xiao, J. LSUN: construction of a large-scale image dataset using deep learning with humans in the loop. *CoRR*, abs/1506.03365, 2015. URL <http://arxiv.org/abs/1506.03365>.
- Zhang, J., Xu, Z., Cui, S., Meng, C., Wu, W., and Lyu, M. R. On the robustness of latent diffusion models. *CoRR*, abs/2306.08257, 2023a. doi: 10.48550/ARXIV.2306.08257. URL <https://doi.org/10.48550/arXiv.2306.08257>.
- Zhang, Y., Hu, S., Zhang, L., Shi, J., Li, M., Liu, X., Wan, W., and Jin, H. Why does little robustness help? a further step towards understanding adversarial transferability, 07 2023b.
- Zhao, Z., Liu, Z., and Larson, M. A. On success and simplicity: A second look at transferable targeted attacks. In Ranzato, M., Beygelzimer, A., Dauphin,

Y. N., Liang, P., and Vaughan, J. W. (eds.), *Advances in Neural Information Processing Systems 34: Annual Conference on Neural Information Processing Systems 2021, NeurIPS 2021, December 6-14, 2021, virtual*, pp. 6115–6128, 2021. URL <https://proceedings.neurips.cc/paper/2021/hash/30d454f09b771b9f65e3eaf6e00fa7bd-Abstract.html>.

A. Experimental Setups

A.1. Setups for Section 3.3

The LDMs we choose are SD-v1-4², SD-v1-5³, and SD-v2-1⁴. We choose the dataset released by Zhang et al. (2023a) to perform our experiments. AEs are all generated by l_∞ PGD (Madry et al., 2018) with $\varepsilon = 8/255$, steps = 40, and step size = $1/255$, which is of the same setting as Liang et al. (2023).

A.2. Setups for Section 4

A.2.1. DATASETS

We use the dataset released by Zhang et al. (2023a) to perform our experiments on image variation task and image inpainting task. This dataset contains 100 images for each task, and each image has 5 prompts for generation. The resolution of each image is 512×512 .

Following Liang et al. (2023), we choose LSUN-airplane and LSUN-cat (Yu et al., 2015) for textual inversion. Observing that LSUN-airplane and LSUN-cat are noisy, where airplane debris and texts are also included, we use CLIP (Bianchi et al., 2021) to choose 200 high-quality images. For example, we calculate the similarity between the prompt “cat” and images in LSUN-cat and choose the top-200 images having higher similarity to the prompt. Lastly, we resize and center crop the image to 256×256 .

A.2.2. LDMs

We use SD-v1-4², SD-v1-5³, and SD-v2-1⁴ as our surrogate models for generating MC-based (Liang et al., 2023; Xue et al., 2023) and encoder-based AEs (Liang & Wu, 2023). Apart from the above three LDMs, we use SD-Inpainting⁵ and SD-2-Inpainting⁶ to generate chain-based AEs (Zhang et al., 2023a) for image inpainting, which is of the same setting to Zhang et al. (2023a).

We use SD-v1-4, SD-v1-5, SD-v2-1, and InstructPix2Pix⁷ as target models for image variation. We use SD-Inpainting⁵ and SD-2-Inpainting⁶ as target models for image inpainting.

We use SD-v1-5 to conduct textual inversion.

A.2.3. BASELINES

We choose three types of adversarial attack as our baselines.

We choose AdvDM (Liang et al., 2023) and SDS with gradient descent (Xue et al., 2023) to represent the MC-based adversarial attack. For the encoder-based adversarial attack, we choose Mist (Liang & Wu, 2023) with the same target image provided by Liang & Wu (2023). For the chain-based adversarial attack, we choose the algorithm proposed by Zhang et al. (2023a), which can be seen as an elaborately tuned photoguard (Salman et al., 2023).

AdvDM_a^b represents AdvDM that samples time steps t from $u(a+1, b)$, and AdvDM = AdvDM₀¹⁰⁰⁰. Mist’s loss includes Equation (3) and Equation (5) and multiplies Equation (5) by a fuse weight w , which can be seen as a combination of the encoder-based attack and AdvDM. For conciseness, we denote Mist (w) as Mist with fuse weight w wherein Mist (0) is a pure encoder-based attack. We also try to use our modified AdvDM to replace the vanilla AdvDM in Mist and denote Mist_a^b(w) as the combination of the encoder-based attack and AdvDM_a^b with fuse weight w .

Considering only one chain-based attack is included, we denote the algorithm proposed by Zhang et al. (2023a) as *Chain*.

²<https://huggingface.co/CompVis/stable-diffusion-v-1-4-original>

³<https://huggingface.co/runwayml/stable-diffusion-v1-5>

⁴<https://huggingface.co/stabilityai/stable-diffusion-2-1>

⁵<https://huggingface.co/runwayml/stable-diffusion-inpainting>

⁶<https://huggingface.co/stabilityai/stable-diffusion-2-inpainting>

⁷<https://huggingface.co/timbrooks/instruct-pix2pix>

A.2.4. HYPER-PARAMETERS OF ADVERSARIAL ATTACKS

All adversarial attacks use l_∞ PGD (Madry et al., 2018) to optimize the adversarial perturbation. We set perturbation budget $\varepsilon = 8/255$, iteration steps to 40, and step size to $1/255$. Following the guidelines in the repository of Liang & Wu (2023), we set the fuse weight of Mist to 1 and 5. As for Chain, Zhang et al. (2023a) claimed that including more denoising steps can improve the performance of AEs. We gradually increase the denoising steps and find that we can, at most, include 5 denoising steps on a single A100 40GB. The rest of the settings of Chain is the same as the optimum setting provided by Zhang et al. (2023a). Note that Zhang et al. (2023a) found attacking the encoder is the optimum for constructing AEs for image inpainting, which makes Chain an encoder-based adversarial attack.

A.2.5. HYPER-PARAMETERS OF IMAGE GENERATION

We use diffusers (von Platen et al., 2022) to conduct image variation and inpainting. Following Zhang et al. (2023a) and Salman et al. (2023), we set edit strength to 0.7, denoising steps to 100, and guidance scale to 7.5. InstructPix2Pix does not have the edit strength, and we set denoising steps to 100 and guidance scale to 7.5, which is the default setting provided by diffusers (von Platen et al., 2022).

The script of textual inversion is also provided by diffusers (von Platen et al., 2022). We partition 200 images into 40 5-image groups and obtain 40 pseudo words S^* . We set the batch size to 4 and left the rest of the parameters as default. After fine-tuning the pseudo word S^* , we use the prompt “a good photo of a <sks>” to generate 50 images per pseudo word S^* and acquire 2000 images.

A.2.6. METRICS

Following Zhang et al. (2023a), we use FID (Heusel et al., 2017) to measure the distributional discrepancy between the generated images and the original images. High FID means that the distribution of the generated images is far from the distribution of the original images and that the adversary fails to conduct imitations.

Apart from preventing imitations, we can also corrupt the image variation and inpainting by degrading the generated images’ quality, making the generated images noisy or unnatural. To measure the quality of the generated images, we use Inception Score (IS) (Salimans et al., 2016) and CLIP-IQA (Wang et al., 2023). Specifically, the prompt pairs used in CLIP-IQA are “‘Clean photo’ vs ‘Noisy photo.’” and “‘Natural photo.’ vs ‘Synthetic photo.’”. Lower values of IS and CLIP-IQA mean worse quality of the generated images.

Lastly, since the adversary uses prompts to edit the image, we also use CLIP (Bianchi et al., 2021) to measure the similarity between the prompt and the generated image. Lower CLIP values mean the semantics of the generated image fails to meet the adversary’s need.

B. Proof of Theorem 3.7

First, we provide a lemma that we will use for the proof of Theorem 3.7.

Lemma B.1. *For arbitrary vectors δ , x , and y , suppose $\|\delta\|_2 \leq \varepsilon$, $\|x\|_2 = \|y\|_2 = 1$, and $c \in \mathbb{R}$. We have*

$$\delta \cdot y \leq c - \varepsilon \sqrt{2 - 2 \cos \langle x, y \rangle} \Rightarrow \delta \cdot x \leq c, \quad (13)$$

where $\cos \langle x, y \rangle = \frac{x \cdot y}{\|x\|_2 \cdot \|y\|_2}$.

Proof. $\delta \cdot x = \delta \cdot y + \delta \cdot (x - y) \leq c - \varepsilon \sqrt{2 - 2 \cos \langle x, y \rangle} + \delta \cdot (x - y)$. Applying the law of cosine, we have $\delta \cdot (x - y) \leq \|\delta\|_2 \cdot \|x - y\|_2 \leq \varepsilon \sqrt{2 - 2 \cos \langle x, y \rangle}$. Thus, $\delta \cdot x \leq c$. \square

Below, we provide the proof of Theorem 3.7. The main differences between ours and Yang et al. (2021); Zhang et al. (2023b) lie in Equation (25) and Equation (29), which are derived from Definition 3.3 and Definition 3.6.

Proof. First, we define two auxiliary functions f and g such that

$$f(x, y) = \frac{L_1 - \mathcal{L}_{\mathcal{F}}(x, y) - \beta\varepsilon^2/2}{\|\nabla_x \mathcal{L}_{\mathcal{F}}(x, y)\|_2}, \quad (14)$$

$$g(x, y) = \frac{L_2 - \mathcal{L}_{\mathcal{G}}(x, y) + \beta\varepsilon^2/2}{\|\nabla_x \mathcal{L}_{\mathcal{G}}(x, y)\|_2}. \quad (15)$$

Recall Equation (7) and Equation (8). We have $c_{\mathcal{F}} = \min_{x \in \mathcal{X}} f(x, y)$ and $c_{\mathcal{G}} = \max_{x \in \mathcal{X}} g(x, y)$.

From Definition 3.6, we have

$$\Pr(T(F, G, x, y_1, y_2) = 1) \quad (16)$$

$$= \Pr(\mathcal{L}_{\mathcal{F}}(x, y_1) \leq L_1 \wedge \mathcal{L}_{\mathcal{G}}(x, y_2) \leq L_2 \wedge \mathcal{L}_{\mathcal{F}}(x', y_1) > L_1 \wedge \mathcal{L}_{\mathcal{G}}(x', y_2) > L_2) \quad (17)$$

$$= 1 - \Pr(\mathcal{L}_{\mathcal{F}}(x, y_1) > L_1 \vee \mathcal{L}_{\mathcal{G}}(x, y_2) > L_2 \vee \mathcal{L}_{\mathcal{F}}(x', y_1) \leq L_1 \vee \mathcal{L}_{\mathcal{G}}(x', y_2) \leq L_2) \quad (18)$$

$$\geq 1 - \Pr(\mathcal{L}_{\mathcal{F}}(x, y_1) > L_1) - \Pr(\mathcal{L}_{\mathcal{G}}(x, y_2) > L_2) - \Pr(\mathcal{L}_{\mathcal{F}}(x', y_1) \leq L_1) - \Pr(\mathcal{L}_{\mathcal{G}}(x', y_2) \leq L_2) \quad (19)$$

$$\geq (1 - \alpha) - (\gamma_{\mathcal{F}} + \gamma_{\mathcal{G}}) - \Pr(\mathcal{L}_{\mathcal{G}}(x', y_2) \leq L_2), \quad (20)$$

where $x' = x + \delta$, Equation (19) is derived from the principle of inclusion-exclusion, and Equation (20) is derived from Definition 3.4 and Definition 3.3.

Applying Taylor's Theorem with Lagrange remainder, we have

$$\mathcal{L}_{\mathcal{F}}(x + \delta, y_1) = \mathcal{L}_{\mathcal{F}}(x, y_1) + \delta \nabla_x \mathcal{L}_{\mathcal{F}}(x, y_1) + \frac{1}{2} \xi^T \mathbf{H}_{\mathcal{F}} \xi, \quad (21)$$

$$\mathcal{L}_{\mathcal{G}}(x + \delta, y_2) = \mathcal{L}_{\mathcal{G}}(x, y_2) + \delta \nabla_x \mathcal{L}_{\mathcal{G}}(x, y_2) + \frac{1}{2} \xi^T \mathbf{H}_{\mathcal{G}} \xi, \quad (22)$$

where $\xi = k\delta$ with $k \in [0, 1]$, and $\mathbf{H}_{\mathcal{F}}$ and $\mathbf{H}_{\mathcal{G}}$ are Hessian matrices of $\mathcal{L}_{\mathcal{F}}(x, y_1)$ and $\mathcal{L}_{\mathcal{G}}(x, y_2)$ respectively. Since both F and G are β -smooth, the maximum eigenvalues of $\mathbf{H}_{\mathcal{F}}$ and $\mathbf{H}_{\mathcal{G}}$ are bounded by β . Thus, we have $|\xi^T \mathbf{H} \xi| \leq \beta \|\xi\|_2^2 \leq \beta\varepsilon^2$. With this inequality, we have

$$\mathcal{L}_{\mathcal{F}}(x, y_1) + \delta \nabla_x \mathcal{L}_{\mathcal{F}}(x, y_1) - \frac{1}{2} \beta\varepsilon^2 \leq \mathcal{L}_{\mathcal{F}}(x + \delta, y_1) \leq \mathcal{L}_{\mathcal{F}}(x, y_1) + \delta \nabla_x \mathcal{L}_{\mathcal{F}}(x, y_1) + \frac{1}{2} \beta\varepsilon^2, \quad (23)$$

$$\mathcal{L}_{\mathcal{G}}(x, y_2) + \delta \nabla_x \mathcal{L}_{\mathcal{G}}(x, y_2) - \frac{1}{2} \beta\varepsilon^2 \leq \mathcal{L}_{\mathcal{G}}(x + \delta, y_2) \leq \mathcal{L}_{\mathcal{G}}(x, y_2) + \delta \nabla_x \mathcal{L}_{\mathcal{G}}(x, y_2) + \frac{1}{2} \beta\varepsilon^2, \quad (24)$$

Applying the right side of Equation (23), we have

$$\Pr(\mathcal{L}_{\mathcal{F}}(x + \delta, y_1) \leq L_1) \quad (25)$$

$$\geq \Pr(\mathcal{L}_{\mathcal{F}}(x, y_1) + \delta \nabla_x \mathcal{L}_{\mathcal{F}}(x, y_1) + \frac{1}{2} \beta\varepsilon^2 \leq L_1) \quad (26)$$

$$= \Pr\left(\delta \cdot \frac{\nabla_x \mathcal{L}_{\mathcal{F}}(x, y_1)}{\|\nabla_x \mathcal{L}_{\mathcal{F}}(x, y_1)\|_2} \leq f(x, y_1)\right), \quad (27)$$

and thus

$$\Pr(\mathcal{L}_{\mathcal{F}}(x + \delta, y_1) \leq L_1) \leq \alpha \Rightarrow \Pr\left(\delta \cdot \frac{\nabla_x \mathcal{L}_{\mathcal{F}}(x, y_1)}{\|\nabla_x \mathcal{L}_{\mathcal{F}}(x, y_1)\|_2} \leq f(x, y_1)\right) \leq \alpha. \quad (28)$$

Similarly, apply the left side of Equation (24) to $\Pr(\mathcal{L}_{\mathcal{G}}(x', y_2) \leq L_2)$:

$$\Pr(\mathcal{L}_{\mathcal{G}}(x', y_2) \leq L_2) \quad (29)$$

$$\leq \Pr(\mathcal{L}_{\mathcal{G}}(x, y_2) + \delta \nabla_x \mathcal{L}_{\mathcal{G}}(x, y_2) - \frac{1}{2} \beta\varepsilon^2 \leq L_2) \quad (30)$$

$$= \Pr\left(\delta \cdot \frac{\nabla_x \mathcal{L}_{\mathcal{G}}(x, y_2)}{\|\nabla_x \mathcal{L}_{\mathcal{G}}(x, y_2)\|_2} \leq g(x, y_2)\right) \quad (31)$$

$$\leq \Pr\left(\delta \cdot \frac{\nabla_x \mathcal{L}_{\mathcal{G}}(x, y_2)}{\|\nabla_x \mathcal{L}_{\mathcal{G}}(x, y_2)\|_2} \leq c_{\mathcal{G}}\right). \quad (32)$$

Note that $\|\delta\| \leq \varepsilon$ and that both $\frac{\nabla_x \mathcal{L}_{\mathcal{F}}(x, y_1)}{\|\nabla_x \mathcal{L}_{\mathcal{F}}(x, y_1)\|_2}$ and $\frac{\nabla_x \mathcal{L}_{\mathcal{G}}(x, y_2)}{\|\nabla_x \mathcal{L}_{\mathcal{G}}(x, y_2)\|_2}$ are unit vectors. Consequently, we apply Lemma B.1 and deduce

$$\delta \cdot \frac{\nabla_x \mathcal{L}_{\mathcal{G}}(x, y_2)}{\|\nabla_x \mathcal{L}_{\mathcal{G}}(x, y_2)\|_2} \leq f(x, y_1) - \varepsilon \sqrt{2 - 2\mathcal{S}(\mathcal{L}_{\mathcal{F}}, \mathcal{L}_{\mathcal{G}}, x, y_1, y_2)} \quad (33)$$

$$\Rightarrow \delta \cdot \frac{\nabla_x \mathcal{L}_{\mathcal{G}}(x, y_2)}{\|\nabla_x \mathcal{L}_{\mathcal{G}}(x, y_2)\|_2} \leq f(x, y_1) - \varepsilon \sqrt{2 - 2 \cos \langle \nabla_x \mathcal{L}_{\mathcal{F}}(x, y_1), \nabla_x \mathcal{L}_{\mathcal{G}}(x, y_2) \rangle} \quad (34)$$

$$\Rightarrow \delta \cdot \frac{\nabla_x \mathcal{L}_{\mathcal{F}}(x, y_1)}{\|\nabla_x \mathcal{L}_{\mathcal{F}}(x, y_1)\|_2} \leq f(x, y_1) \quad (35)$$

$$\Rightarrow \Pr\left(\delta \cdot \frac{\nabla_x \mathcal{L}_{\mathcal{G}}(x, y_2)}{\|\nabla_x \mathcal{L}_{\mathcal{G}}(x, y_2)\|_2} \leq f(x, y_1) - \varepsilon \sqrt{2 - 2\mathcal{S}(\mathcal{L}_{\mathcal{F}}, \mathcal{L}_{\mathcal{G}}, x, y_1, y_2)}\right) \leq \Pr\left(\delta \cdot \frac{\nabla_x \mathcal{L}_{\mathcal{F}}(x, y_1)}{\|\nabla_x \mathcal{L}_{\mathcal{F}}(x, y_1)\|_2} \leq f(x, y_1)\right) \leq \alpha. \quad (36)$$

Since $c_{\mathcal{F}} = \min_{x \in \mathcal{X}} f(x, y_1) \leq f(x, y_1)$, we have

$$\Pr\left(\delta \cdot \frac{\nabla_x \mathcal{L}_{\mathcal{G}}(x, y_2)}{\|\nabla_x \mathcal{L}_{\mathcal{G}}(x, y_2)\|_2} \leq c_{\mathcal{F}} - \varepsilon \sqrt{2 - 2\mathcal{S}(\mathcal{L}_{\mathcal{F}}, \mathcal{L}_{\mathcal{G}}, x, y_1, y_2)}\right) \leq \alpha. \quad (37)$$

Note that $\delta \cdot \frac{\nabla_x \mathcal{L}_{\mathcal{G}}(x, y_2)}{\|\nabla_x \mathcal{L}_{\mathcal{G}}(x, y_2)\|_2} \geq -\varepsilon$. Thus, its expectation is bounded:

$$\mathbb{E}\left[\delta \cdot \frac{\nabla_x \mathcal{L}_{\mathcal{G}}(x, y_2)}{\|\nabla_x \mathcal{L}_{\mathcal{G}}(x, y_2)\|_2}\right] \geq -\varepsilon\alpha + (c_{\mathcal{F}} - \varepsilon \sqrt{2 - 2\mathcal{S}(\mathcal{L}_{\mathcal{F}}, \mathcal{L}_{\mathcal{G}}, x, y_1, y_2)})(1 - \alpha). \quad (38)$$

Applying Markov's inequality and combining Equation (32), we have

$$\Pr(\mathcal{L}_{\mathcal{G}}(x', y_2) \leq L_2) \leq \Pr\left(\delta \cdot \frac{\nabla_x \mathcal{L}_{\mathcal{G}}(x, y_2)}{\|\nabla_x \mathcal{L}_{\mathcal{G}}(x, y_2)\|_2} \leq c_{\mathcal{G}}\right) \leq \frac{\varepsilon(1 + \alpha) - (c_{\mathcal{F}} - \varepsilon \sqrt{2 - 2\mathcal{S}(\mathcal{L}_{\mathcal{F}}, \mathcal{L}_{\mathcal{G}}, x, y_1, y_2)})(1 - \alpha)}{\varepsilon - c_{\mathcal{G}}}, \quad (39)$$

and thus

$$\Pr(T(\mathcal{F}, \mathcal{G}, x, y_1, y_2) = 1) \geq (1 - \alpha) - (\gamma_{\mathcal{F}} + \gamma_{\mathcal{G}}) - \frac{\varepsilon(1 + \alpha) - c_{\mathcal{F}}(1 - \alpha)}{\varepsilon - c_{\mathcal{G}}} - \frac{\varepsilon(1 - \alpha)}{\varepsilon - c_{\mathcal{G}}} \sqrt{2 - 2\mathcal{S}(\mathcal{L}_{\mathcal{F}}, \mathcal{L}_{\mathcal{G}}, x, y_1, y_2)} \quad (40)$$

□

C. Additional Results Demonstrating Smoothness can Boost AEs for LDMs

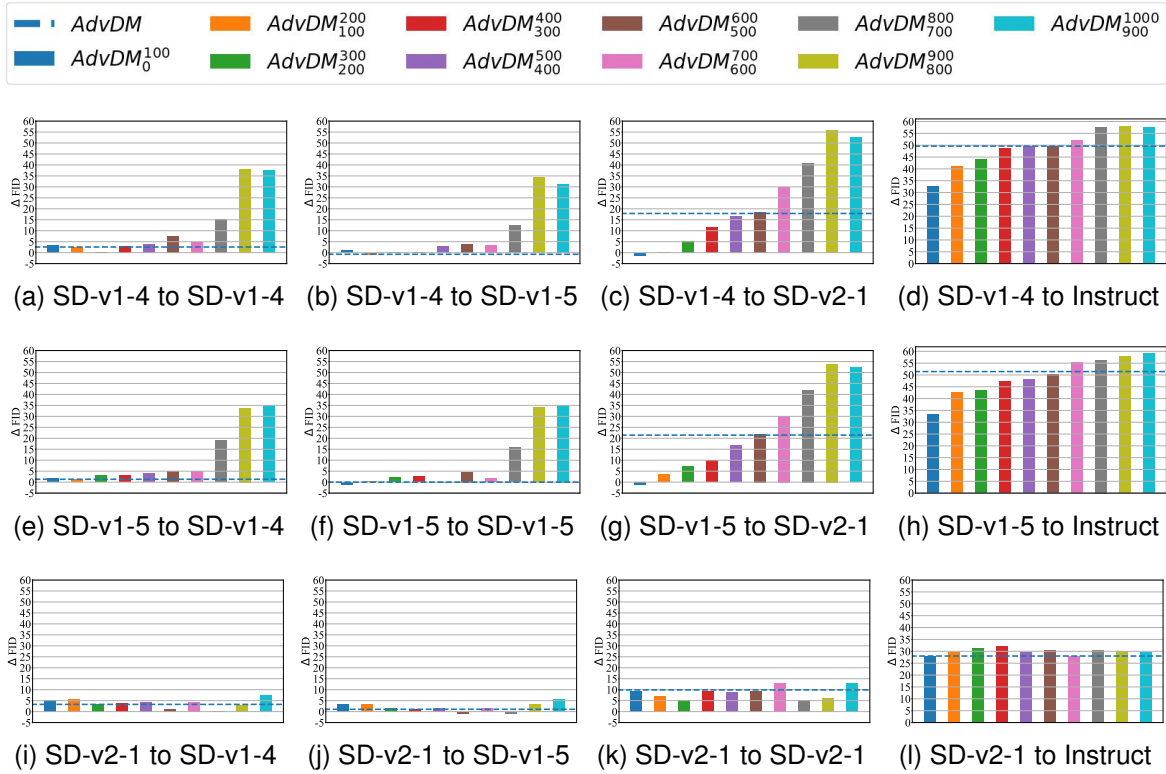


Figure 6. The increments \uparrow of FID relative to the benign’s. Larger increment means worse generated images and better AEs for image variation task. “A to B” means that AEs are generated by A and attack B.

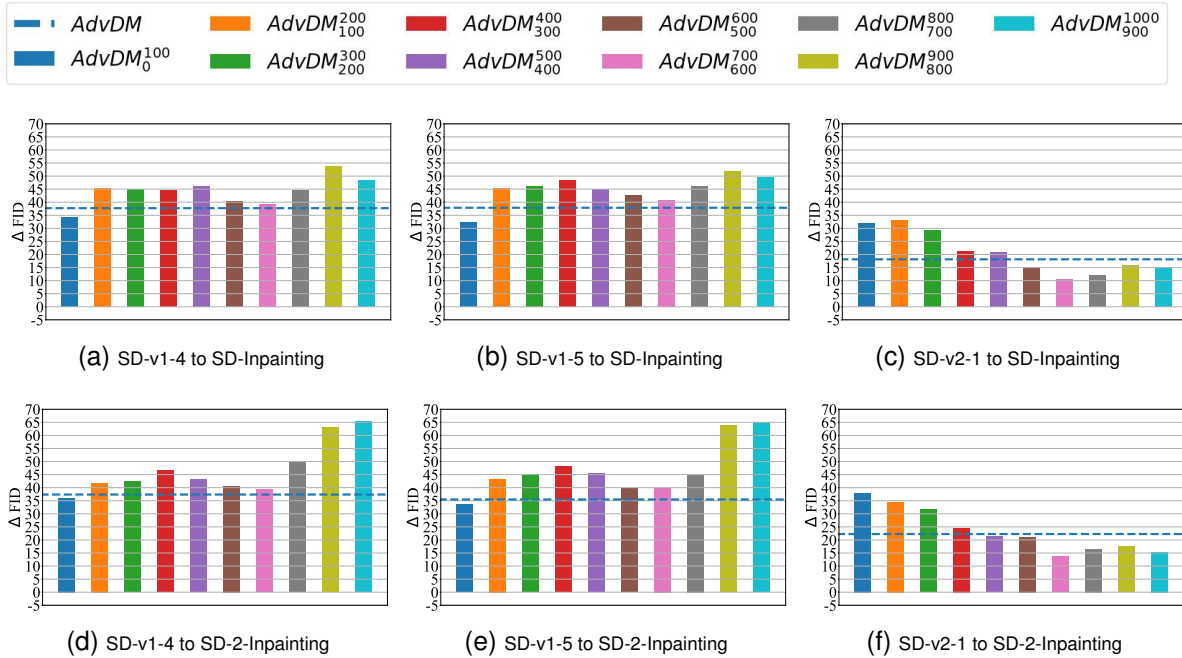


Figure 7. The increments \uparrow of FID relative to the benign’s. Larger increment means worse generated images and better AEs for image inpainting task. “A to B” means that AEs are generated by A and attack B.

D. Results with SD-v1-5 being the Surrogate Model

Table 5. The performance of AEs in corrupting image variation. The best result in each column is in **bold**.

Surrogate Model	Method	FID \uparrow				IS \downarrow				CLIP \downarrow				CLIP-IQA (Natural) \downarrow				CLIP-IQA (Noisiness) \downarrow			
		SD-v1-4	SD-v1-5	SD-v2-1	Instruct	SD-v1-4	SD-v1-5	SD-v2-1	Instruct	SD-v1-4	SD-v1-5	SD-v2-1	Instruct	SD-v1-4	SD-v1-5	SD-v2-1	Instruct	SD-v1-4	SD-v1-5	SD-v2-1	Instruct
SD-v1-5	AdvDM	165.60	166.50	217.27	181.85	15.85	15.64	9.74	15.34	34.67	34.57	30.96	34.29	0.45	0.45	0.19	0.22	0.44	0.44	0.28	0.39
	SDS	175.04	176.68	210.96	158.57	16.91	16.17	11.24	14.94	34.42	34.31	31.83	34.15	0.43	0.42	0.23	0.23	0.46	0.46	0.33	0.31
	Chain	174.58	172.95	211.11	157.83	15.02	14.41	9.88	16.62	34.28	34.37	31.43	34.55	0.39	0.39	0.18	0.23	0.44	0.45	0.31	0.32
	Mist (0)	181.24	181.81	231.18	158.81	16.62	15.04	9.01	15.23	34.12	34.09	30.54	34.01	0.44	0.44	0.21	0.18	0.45	0.46	0.32	0.17
	Mist (1)	180.79	183.68	235.27	157.01	15.93	15.00	9.36	14.71	34.12	34.08	30.44	33.90	0.44	0.44	0.21	0.17	0.46	0.46	0.33	0.17
	Mist (5)	167.58	167.50	216.56	181.35	16.58	15.04	10.02	14.94	34.60	34.56	31.12	34.20	0.45	0.45	0.19	0.22	0.44	0.46	0.28	0.39
	AdvDM $_{800}^{900}$	198.10	200.62	249.66	188.11	11.79	12.69	7.75	15.56	33.70	33.73	29.75	33.95	0.30	0.32	0.09	0.21	0.32	0.33	0.16	0.41
	Mist $_{800}^{900}$ (1)	181.74	180.81	234.47	157.97	16.05	15.26	8.60	15.41	34.13	34.03	30.41	33.97	0.44	0.44	0.19	0.18	0.45	0.47	0.31	0.17
	Mist $_{800}^{900}$ (5)	198.51	202.07	249.01	189.57	11.49	11.96	7.38	14.90	33.67	33.71	29.52	33.88	0.29	0.32	0.09	0.21	0.32	0.33	0.16	0.41

Table 6. The performance of AEs in corrupting image inpainting. The best result in each column is in **bold**.

Surrogate Model	Method	FID \uparrow		IS \downarrow		CLIP \downarrow		CLIP-IQA (Natural) \downarrow		CLIP-IQA (Noisiness) \downarrow	
		SD-Inpainting	SD-2-Inpainting	SD-Inpainting	SD-2-Inpainting	SD-Inpainting	SD-2-Inpainting	SD-Inpainting	SD-2-Inpainting	SD-Inpainting	SD-2-Inpainting
SD-v1-5	AdvDM	145.94	141.29	14.59	14.36	34.32	34.97	0.26	0.28	0.36	0.33
	SDS	145.06	148.10	15.14	15.27	34.59	34.86	0.35	0.34	0.36	0.27
	Mist (0)	155.18	163.12	13.90	14.73	33.99	34.16	0.25	0.21	0.37	0.30
	Mist (1)	155.24	161.80	14.96	14.44	34.04	34.31	0.25	0.22	0.37	0.29
	Mist (5)	146.10	144.39	14.52	14.93	34.28	34.99	0.26	0.27	0.37	0.32
	AdvDM $_{800}^{900}$	159.95	169.59	13.57	12.78	34.34	34.57	0.21	0.21	0.27	0.23
	Mist $_{800}^{900}$ (1)	156.85	161.62	14.61	14.70	34.13	34.14	0.25	0.22	0.37	0.30
	Mist $_{800}^{900}$ (5)	158.79	168.68	13.69	12.69	34.29	34.65	0.21	0.21	0.27	0.23

E. Results of adversarial attacks with 500 iteration steps

We present the results of adversarial attacks with 500 iteration steps in Table 7 and Table 8. Due to the high computation overhead of Chain (Zhang et al., 2023a), it is impossible to conduct Chain with 500 iteration steps.

Table 7. The performance of AEs generated by different methods with 500 iteration steps in cracking image variation. The surrogate model is SD-v1-4.

Method	FID \uparrow				IS \downarrow				CLIP \downarrow				CLIP-IQA (Natural) \downarrow				CLIP-IQA (Noisiness) \downarrow			
	SD-v1-4	SD-v1-5	SD-v2-1	Instruct	SD-v1-4	SD-v1-5	SD-v2-1	Instruct	SD-v1-4	SD-v1-5	SD-v2-1	Instruct	SD-v1-4	SD-v1-5	SD-v2-1	Instruct	SD-v1-4	SD-v1-5	SD-v2-1	Instruct
AdvDM	173.77	171.11	230.73	184.93	15.30	15.17	9.22	15.29	34.47	34.54	30.52	33.95	0.44	0.43	0.18	0.22	0.44	0.45	0.27	0.39
SDS	181.94	179.55	214.01	178.81	16.85	15.61	10.81	15.48	34.17	34.15	31.54	33.65	0.42	0.43	0.22	0.18	0.46	0.47	0.35	0.32
Mist (0)	184.27	183.17	245.44	181.69	15.88	14.83	8.37	14.27	34.07	33.87	29.74	33.32	0.44	0.43	0.18	0.13	0.46	0.47	0.31	0.17
Mist (1)	182.31	186.22	243.68	184.48	16.71	15.68	8.47	13.70	33.97	33.91	29.74	33.27	0.43	0.44	0.18	0.12	0.47	0.48	0.30	0.15
Mist (5)	171.63	172.66	229.18	186.08	15.82	15.74	9.76	15.72	34.41	34.29	30.53	34.00	0.43	0.43	0.16	0.22	0.44	0.45	0.26	0.40
AdvDM $_{800}^{900}$	243.93	242.59	279.78	192.93	7.08	7.71	6.17	14.02	32.39	32.54	28.05	33.82	0.17	0.19	0.05	0.20	0.19	0.19	0.11	0.42

Table 8. The performance of AEs generated by different methods with 500 iteration steps in cracking image inpainting. The surrogate model is SD-v1-4.

Method	FID \uparrow		IS \downarrow		CLIP \downarrow		CLIP-IQA (Natural) \downarrow		CLIP-IQA (Noisiness) \downarrow	
	SD-Inpainting	SD-2-Inpainting	SD-Inpainting	SD-2-Inpainting	SD-Inpainting	SD-2-Inpainting	SD-Inpainting	SD-2-Inpainting	SD-Inpainting	SD-2-Inpainting
AdvDM	155.47	152.80	14.42	14.67	34.24	34.92	0.23	0.25	0.35	0.32
SDS	154.22	156.96	15.89	15.26	34.43	34.61	0.31	0.30	0.31	0.23
Mist (0)	172.52	176.01	13.18	13.84	33.63	33.86	0.22	0.19	0.36	0.29
Mist (1)	171.89	178.58	13.79	14.29	33.73	33.85	0.22	0.18	0.36	0.28
Mist (5)	155.40	150.25	14.86	14.66	34.17	34.96	0.24	0.24	0.35	0.31
AdvDM $_{800}^{900}$	188.28	213.68	10.92	8.51	33.71	33.99	0.17	0.14	0.21	0.15

F. Pre-processing Adversarial Defense

We use JPEG compression (Segura et al., 2023) and TVM (Guo et al., 2018) to test the robustness of AEs generated by different methods (see Table 9). Generally, JPEG can degrade the performance of all methods to the same level since none have considered the robustness of AEs. One intriguing phenomenon in Table 9 is that TVM, being an adversarial defense, even degrades the quality of the generated image, which suggests that disturbance brought by the pre-processing adversarial defense may even boost the performance of AEs for LDMs.

Table 9. The performance of AEs facing different pre-processing adversarial defenses. The surrogate model is SD-v1-4. JPEG (*a*) represents JPEG compression with quality *a*.

Defense	Method	FID↑			IS↓			CLIP↓			CLIP-IQA (Natural)↓				CLIP-IQA (Noisiness)↓						
		SD-v1-4	SD-v1-5	SD-v2-1	Instruct	SD-v1-4	SD-v1-5	SD-v2-1	Instruct	SD-v1-4	SD-v1-5	SD-v2-1	Instruct	SD-v1-4	SD-v1-5	SD-v2-1	Instruct	SD-v1-4	SD-v1-5	SD-v2-1	Instruct
JPEG (85)	AdvDM	166.09	164.73	206.84	171.89	16.25	15.74	10.56	15.57	34.52	34.59	31.60	34.31	0.46	0.46	0.24	0.22	0.45	0.45	0.31	0.37
	SDS	170.51	170.02	203.24	133.20	16.45	15.92	12.12	16.55	34.57	34.61	32.34	34.55	0.43	0.44	0.26	0.30	0.46	0.46	0.36	0.29
	Chain	177.41	176.04	220.79	153.53	13.66	14.12	9.04	16.53	34.05	34.20	30.65	34.58	0.36	0.36	0.15	0.24	0.42	0.43	0.27	0.33
	Mist (0)	174.84	174.81	211.24	133.64	16.27	16.03	10.39	16.14	34.40	34.31	31.51	34.48	0.44	0.45	0.22	0.26	0.46	0.47	0.33	0.24
	Mist (1)	173.76	173.57	217.31	135.33	16.14	15.61	10.15	16.37	34.51	34.57	31.59	34.67	0.45	0.45	0.23	0.26	0.45	0.47	0.33	0.24
	Mist (5)	165.02	166.14	206.60	171.81	16.23	15.79	10.75	15.76	34.67	34.55	31.60	34.32	0.45	0.47	0.24	0.23	0.45	0.46	0.33	0.38
	AdvDM ⁰⁰⁰ ₈₀₀	177.50	178.91	231.19	181.72	14.96	15.06	8.73	15.67	34.41	34.28	30.40	34.03	0.38	0.38	0.14	0.22	0.41	0.41	0.22	0.40
	Mist ⁰⁰⁰ ₈₀₀ (1)	173.11	174.27	212.44	134.38	15.94	15.60	10.38	15.82	34.46	34.42	31.70	34.51	0.45	0.46	0.24	0.25	0.45	0.47	0.34	0.24
	Mist ⁰⁰⁰ ₈₀₀ (5)	178.65	179.96	228.83	180.12	14.65	15.12	9.03	15.20	34.48	34.24	30.32	34.04	0.38	0.39	0.13	0.23	0.41	0.41	0.21	0.40
	JPEG (75)	AdvDM	165.40	165.09	206.95	166.66	16.45	15.46	11.31	16.75	34.56	34.52	31.78	34.38	0.46	0.47	0.27	0.23	0.45	0.46	0.33
SDS		167.17	168.36	200.83	129.91	16.32	16.40	12.21	16.77	34.51	34.62	32.24	34.62	0.45	0.45	0.25	0.31	0.46	0.48	0.36	0.30
Chain		171.84	171.06	215.63	148.18	14.50	14.73	9.65	16.49	34.30	34.41	30.96	34.71	0.39	0.40	0.18	0.26	0.45	0.45	0.30	0.32
Mist (0)		172.01	172.69	206.14	131.94	16.68	15.73	11.23	16.74	34.33	34.50	31.99	34.69	0.45	0.45	0.26	0.28	0.47	0.47	0.35	0.27
Mist (1)		170.70	169.86	206.38	135.30	16.50	15.43	11.08	16.99	34.32	34.50	31.97	34.67	0.46	0.45	0.25	0.27	0.46	0.47	0.34	0.27
Mist (5)		166.51	166.65	201.29	165.70	16.53	15.79	11.31	16.19	34.62	34.62	31.76	34.42	0.46	0.47	0.25	0.23	0.45	0.46	0.33	0.36
AdvDM ⁰⁰⁰ ₈₀₀		171.64	171.97	216.75	171.96	14.99	15.60	9.56	15.50	34.57	34.48	31.08	34.22	0.41	0.41	0.17	0.23	0.43	0.44	0.27	0.39
Mist ⁰⁰⁰ ₈₀₀ (1)		172.39	171.03	208.86	133.40	16.54	15.13	10.51	16.66	34.40	34.52	32.00	34.64	0.46	0.46	0.25	0.28	0.47	0.47	0.33	0.27
Mist ⁰⁰⁰ ₈₀₀ (5)		171.68	171.91	217.01	174.63	15.34	15.43	9.93	15.68	34.56	34.57	31.12	34.29	0.41	0.42	0.16	0.23	0.44	0.44	0.27	0.39
JPEG (65)		AdvDM	166.78	165.42	204.28	165.22	16.37	15.98	11.44	16.78	34.51	34.60	31.79	34.45	0.46	0.47	0.26	0.23	0.45	0.46	0.34
	SDS	166.18	168.42	203.62	133.36	16.22	15.79	11.68	16.90	34.50	34.59	32.02	34.66	0.45	0.45	0.26	0.30	0.47	0.48	0.38	0.30
	Chain	169.69	170.03	211.33	147.95	15.70	15.53	9.84	16.36	34.37	34.48	31.28	34.76	0.41	0.42	0.19	0.26	0.46	0.48	0.32	0.33
	Mist (0)	170.60	171.17	204.06	135.86	17.47	16.11	11.43	16.67	34.46	34.50	32.00	34.74	0.45	0.46	0.26	0.29	0.47	0.49	0.36	0.29
	Mist (1)	170.09	169.28	206.35	136.44	16.61	15.87	11.51	16.63	34.40	34.52	31.98	34.70	0.45	0.45	0.25	0.28	0.48	0.49	0.35	0.28
	Mist (5)	165.74	164.92	199.34	165.08	16.26	15.15	11.28	16.24	34.56	34.52	31.97	34.51	0.46	0.47	0.25	0.23	0.46	0.47	0.34	0.35
	AdvDM ⁰⁰⁰ ₈₀₀	168.03	166.58	215.81	171.55	15.38	15.91	10.05	15.76	34.57	34.57	31.36	34.20	0.43	0.43	0.19	0.23	0.46	0.45	0.29	0.38
	Mist ⁰⁰⁰ ₈₀₀ (1)	169.88	169.93	202.05	136.78	16.89	15.50	11.36	16.61	34.50	34.48	32.06	34.60	0.45	0.46	0.25	0.28	0.47	0.49	0.33	0.28
	Mist ⁰⁰⁰ ₈₀₀ (5)	168.80	167.00	213.81	171.64	15.71	15.26	9.81	15.79	34.57	34.60	31.29	34.24	0.43	0.43	0.19	0.23	0.46	0.47	0.31	0.38
	TVM	AdvDM	173.80	173.91	213.00	150.90	15.11	14.95	9.71	15.24	33.99	33.96	31.10	34.17	0.43	0.43	0.27	0.21	0.43	0.44	0.31
SDS		175.08	175.35	215.86	149.69	15.50	15.73	9.76	15.88	33.99	34.09	30.80	34.14	0.43	0.43	0.25	0.25	0.47	0.47	0.31	0.32
Chain		176.11	175.96	222.36	148.43	14.17	14.78	8.77	15.72	33.99	33.90	30.66	34.19	0.41	0.41	0.23	0.24	0.44	0.44	0.27	0.32
Mist (0)		177.01	176.85	225.51	147.70	15.12	15.82	8.31	15.89	33.88	34.01	30.47	34.14	0.43	0.42	0.24	0.23	0.46	0.46	0.29	0.30
Mist (1)		176.23	177.80	226.19	149.39	14.95	15.55	9.12	15.30	33.81	33.97	30.60	34.15	0.43	0.42	0.24	0.23	0.46	0.46	0.29	0.30
Mist (5)		172.80	174.49	213.84	151.58	14.80	14.88	9.87	15.15	33.95	33.96	31.14	34.17	0.43	0.42	0.27	0.21	0.44	0.43	0.31	0.28
AdvDM ⁰⁰⁰ ₈₀₀		171.16	173.60	215.45	154.71	15.20	15.82	9.92	14.90	34.07	34.03	31.25	34.23	0.43	0.44	0.27	0.23	0.44	0.44	0.31	0.30
Mist ⁰⁰⁰ ₈₀₀ (1)		177.29	177.80	222.25	149.47	15.11	15.03	9.04	15.42	33.85	33.97	30.64	34.12	0.42	0.42	0.23	0.24	0.45	0.46	0.29	0.30
Mist ⁰⁰⁰ ₈₀₀ (5)		170.84	173.36	213.76	154.74	14.71	15.60	9.44	14.53	34.03	34.05	31.23	34.19	0.43	0.43	0.27	0.23	0.43	0.44	0.31	0.30

G. More Visualizations

We post more visualizations of images generated with benign images and AEs. The surrogate model used to manufacture AEs for image variation is SD-v1-4. When attacking SD-Inpainting and SD-2-Inpainting, Chain (Zhang et al., 2023a) uses SD-Inpainting and SD-2-Inpainting as surrogate models, respectively. Other adversarial attacks use SD-v1-4 as their surrogate model.

G.1. Attacking SD-v1-4

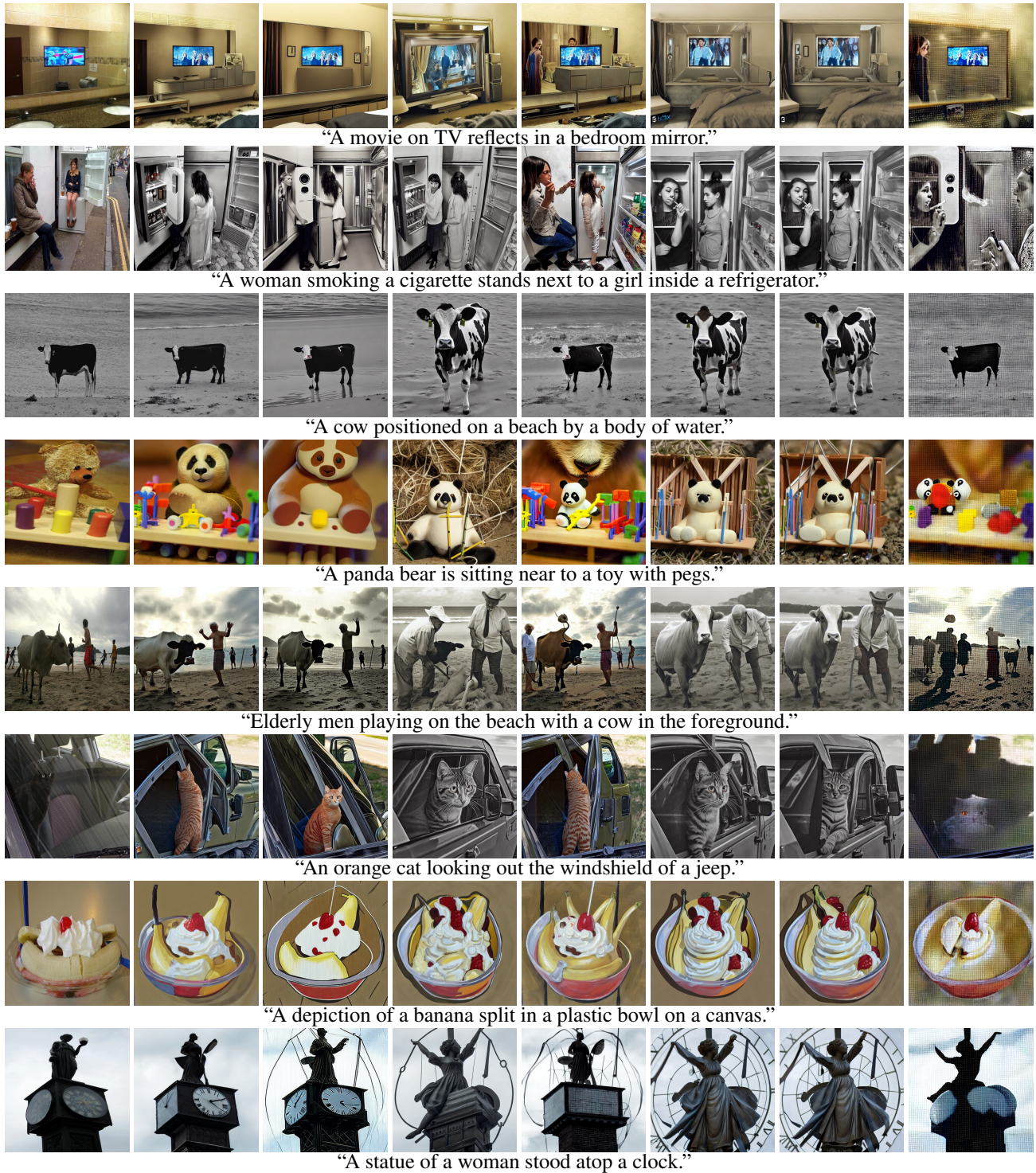


Figure 8. From left to right: Original images, Benign, Chain (Zhang et al., 2023a), SDS (Xue et al., 2023), AdvDM (Liang et al., 2023), Mist (0) (Liang & Wu, 2023), Mist (1) (Liang & Wu, 2023), AdvDM₈₀₀⁹⁰⁰ (Ours). View this figure in color. Use zoom-in to check the texture.

G.2. Attacking SD-v1-5

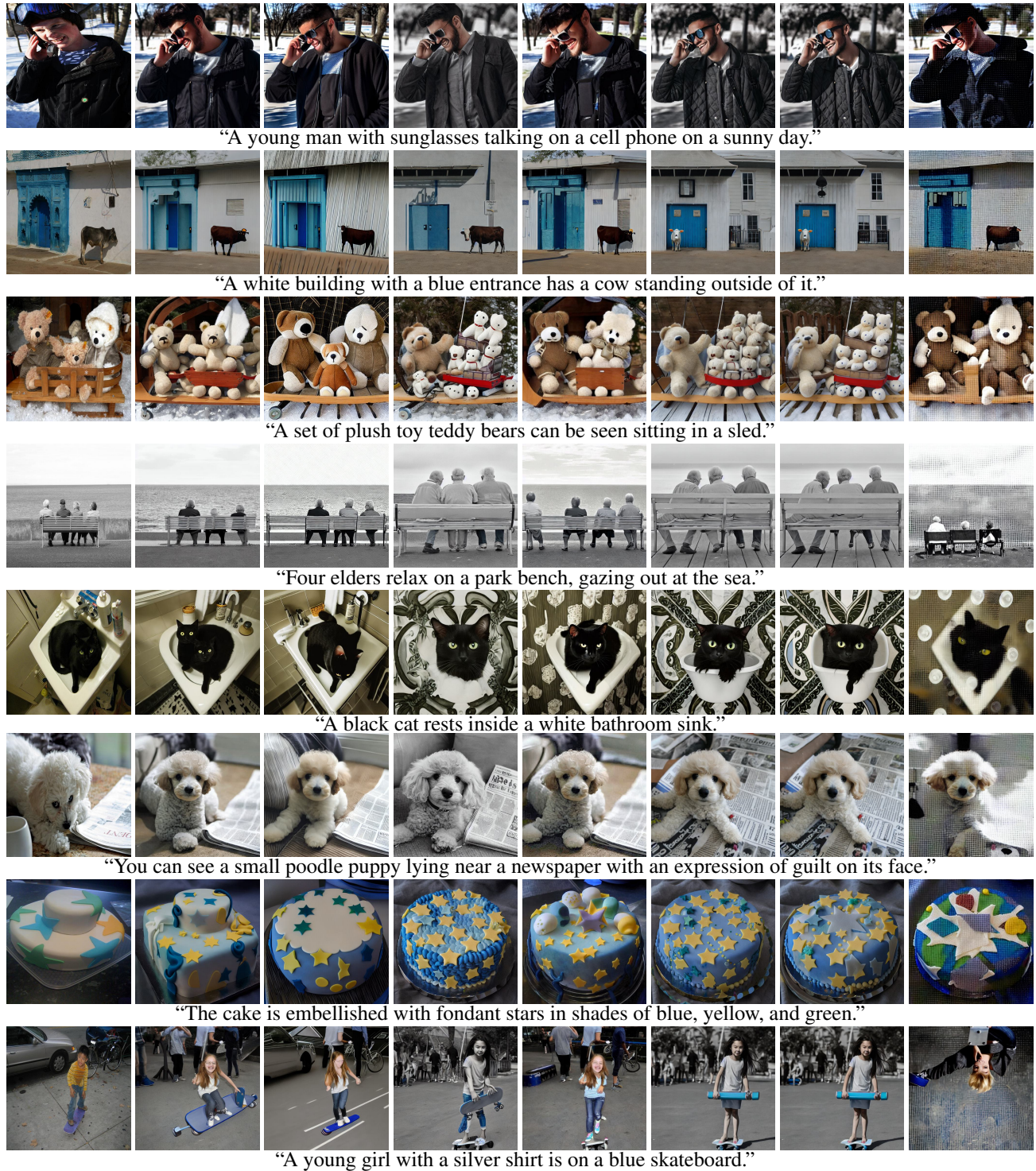


Figure 9. From left to right: Original images, Benign, Chain (Zhang et al., 2023a), SDS (Xue et al., 2023), AdvDM (Liang et al., 2023), Mist (0) (Liang & Wu, 2023), Mist (1) (Liang & Wu, 2023), AdvDM₈₀₀⁹⁰⁰ (Ours). View this figure in color. Use zoom-in to check the texture.

G.3. Attacking SD-v2-1

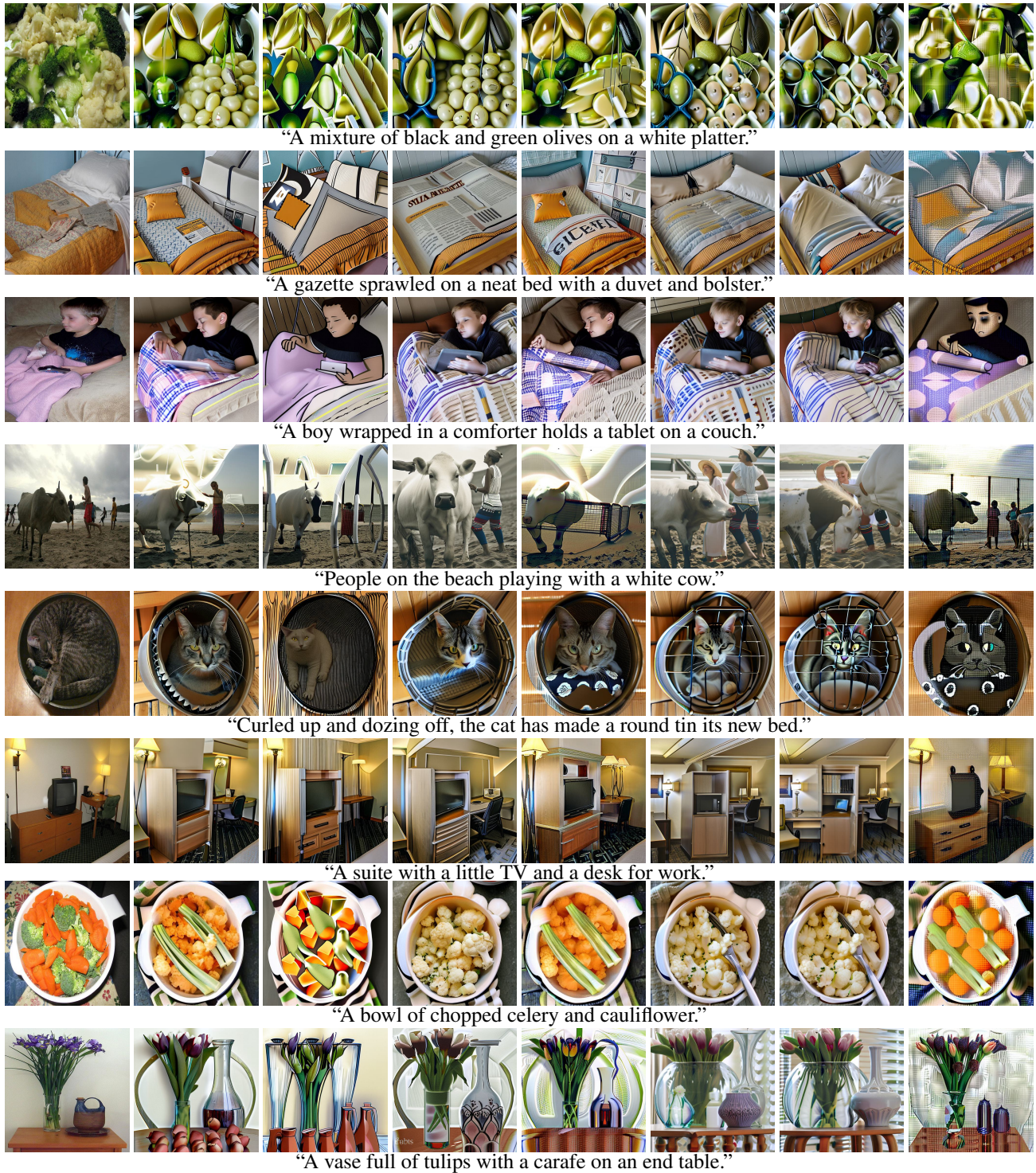


Figure 10. From left to right: Original images, Benign, Chain (Zhang et al., 2023a), SDS (Xue et al., 2023), AdvDM (Liang et al., 2023), Mist (0) (Liang & Wu, 2023), Mist (1) (Liang & Wu, 2023), AdvDM₈₀₀⁹⁰⁰ (Ours). View this figure in color. Use zoom-in to check the texture.

G.4. Attacking InstructPix2Pix

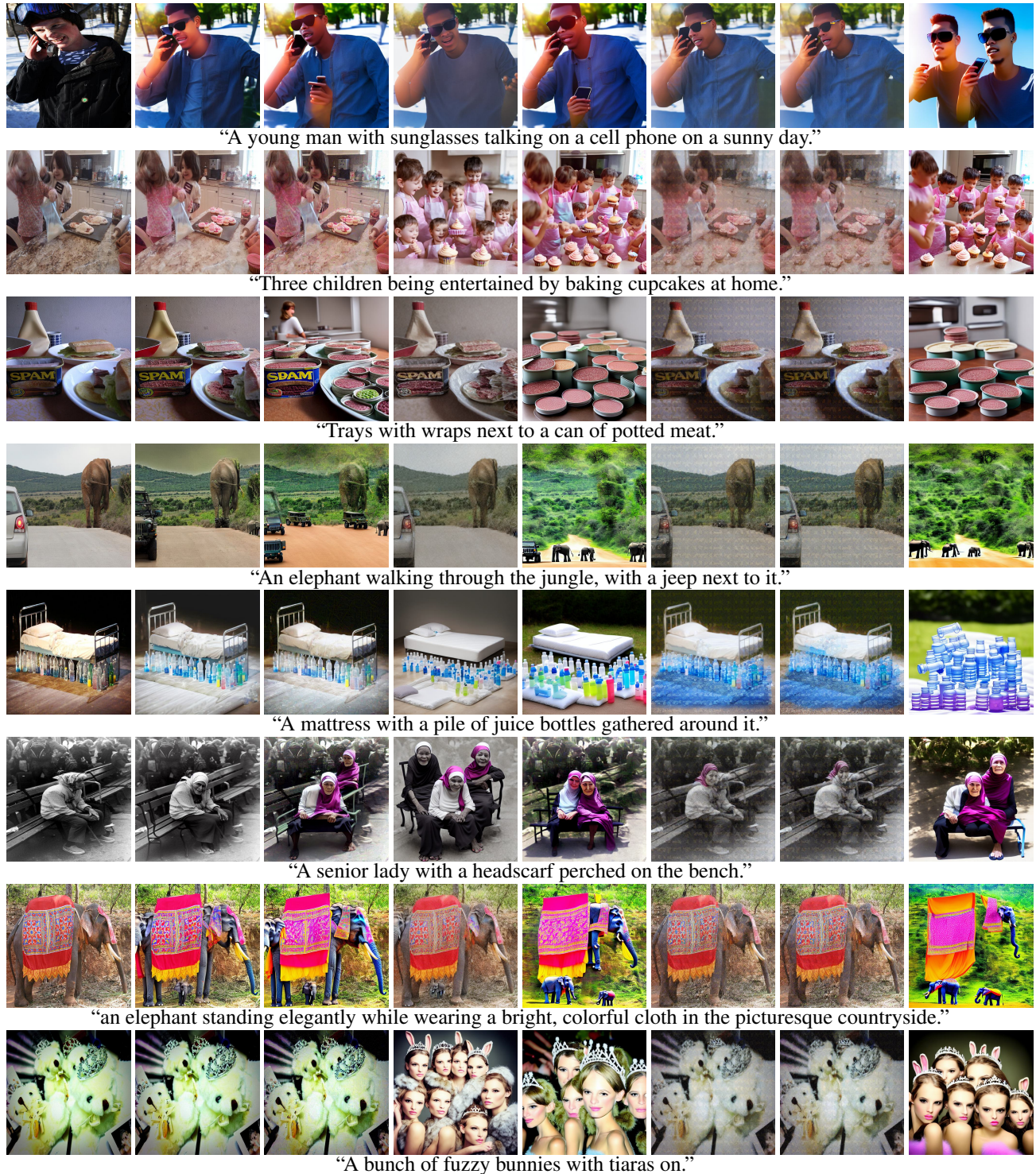


Figure 11. From left to right: Original images, Benign, Chain (Zhang et al., 2023a), SDS (Xue et al., 2023), AdvDM (Liang et al., 2023), Mist (0) (Liang & Wu, 2023), Mist (1) (Liang & Wu, 2023), AdvDM₈₀₀⁹⁰⁰ (Ours). View this figure in color. Use zoom-in to check the texture.

G.5. Attacking SD-Inpainting

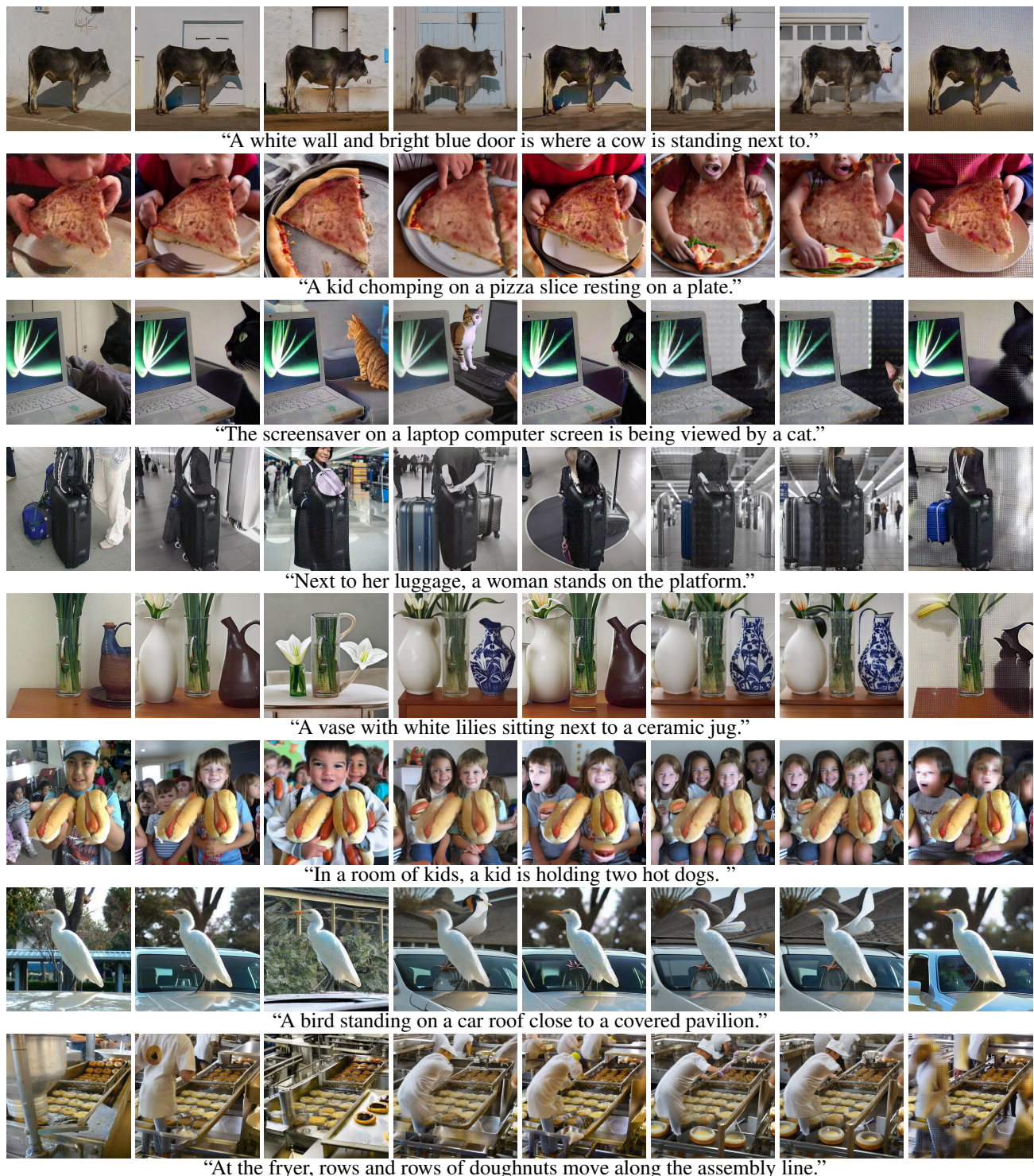


Figure 12. From left to right: Original images, Benign, Chain (Zhang et al., 2023a), SDS (Xue et al., 2023), AdvDM (Liang et al., 2023), Mist (0) (Liang & Wu, 2023), Mist (1) (Liang & Wu, 2023), AdvDM₈₀₀⁹⁰⁰ (Ours). View this figure in color. Use zoom-in to check the texture.

G.6. Attacking SD-2-Inpainting

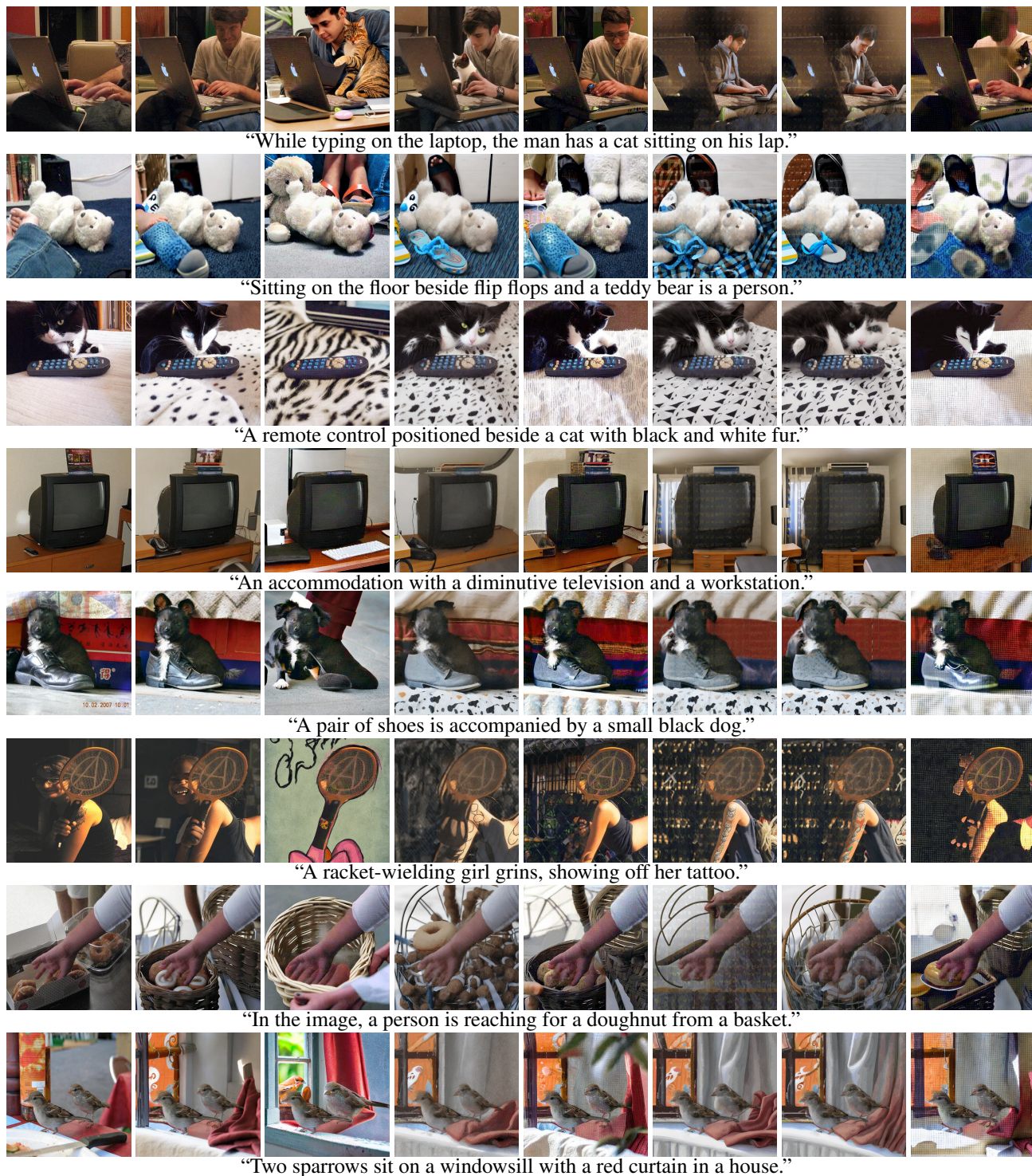


Figure 13. From left to right: Original images, Benign, Chain (Zhang et al., 2023a), SDS (Xue et al., 2023), AdvDM (Liang et al., 2023), Mist (0) (Liang & Wu, 2023), Mist (1) (Liang & Wu, 2023), AdvDM₈₀₀⁹⁰⁰ (Ours). View this figure in color. Use zoom-in to check the texture.